

Original papers

Effects of global climate change on the hydrological cycle and crop growth under heavily irrigated management – A comparison between CMIP5 and CMIP6

Xinlin Li ^{a,b,1}, Lili Tan ^{a,c,1}, Yingxuan Li ^{a,b}, Junyu Qi ^d, Puyu Feng ^{a,b}, Baoguo Li ^{a,b}, De Li Liu ^{e,f}, Xueliang Zhang ^{a,c}, Gray W. Marek ^g, Yingqi Zhang ^{a,c}, Haipeng Liu ^{a,b}, Raghavan Srinivasan ^h, Yong Chen ^{a,c,*}

^a College of Land Science and Technology, China Agricultural University, Beijing 100193, China

^b Key Laboratory of Arable Land Conservation in North China, Ministry of Agriculture and Rural Affairs, Beijing 100193, China

^c Research Center of Land Use and Management, China Agricultural University, Beijing 100193, China

^d Earth System Science Interdisciplinary Center, University of Maryland, College Park, MD 20740, USA

^e NSW Department of Primary Industries, Wagga Wagga Agricultural Institute, Wagga Wagga, NSW 2650, Australia

^f Climate Change Research Centre, University of New South Wales, Sydney 2052, Australia

^g USDA-ARS Conservation and Production Research Laboratory, Bushland, TX 79012, USA

^h Department of Ecosystem Science and Management, Texas A&M University, College Station, TX 77843, USA



ARTICLE INFO

Keywords:

Hydrological modeling

SWAT-MAD

Future climate change

Double-cropping system

Irrigated farming

ABSTRACT

Quantifying the impact of global climate change on the water cycle and crop production is essential for water resource management and agricultural production planning. This study compared multiple GCM (General Circulation Model) projections of CMIP5 (Coupled Model Intercomparison Project 5) and CMIP6 and further used the selected GCMs to quantify the impact of future climate change on hydrology and crop production under intensive irrigation management in the North China Plain using an improved SWAT model (SWAT-MAD). Taylor's skill score was used firstly to screen out six groups of GCMs with better simulation performance from 10 pairs of homologous GCMs of CMIP5 and CMIP6. The selected GCMs of CMIP5 and CMIP6 were further used to drive SWAT-MAD for a robust evaluation of climate change impacts. Results showed that during winter wheat growing season, average actual evapotranspiration (ET_a) increased by 3%, 3%, 4%, and 5%, respectively, under 2041–2070 RCP4.5, 2041–2070 SSP2-4.5, 2041–2100 RCP4.5, and 2071–2100 SSP2-4.5 scenarios, compared to the historical period (1971–2000). During summer maize growing season, those changes in ET_a were 4%, 2%, –0.2%, and –3%. Predicted future precipitation, air temperatures, and surface runoff could increase, while irrigation could decrease as precipitation increased. The dynamic patterns of leaf area index of winter wheat and summer maize indicated that there is a tendency for early emergence and maturity of both crops in the future, and the daily total biomass elevated with a corresponding increase in final yields. The highest increases in yields of winter wheat and summer maize were 18.9% and 16.7%. The findings not only contribute to enhancing the confidence of future projections using CMIP6 but also facilitate our understanding of the relative uncertainty of GCMs. This study provides technical and data support for pre-selections of GCMs and decision making in best management practices for groundwater conservation and agricultural production.

1. Introduction

The growth of the world's population and consumption level increased the global demand for fossil fuels. Studies have shown that

atmospheric carbon dioxide (CO_2) is one of the major causes of climate change (IPCC, 2014). According to a series of CO_2 emission scenarios published by the IPCC, projected global atmospheric CO_2 concentrations can elevate from the current level of 330 ppm to 800 ppm by the end of

* Corresponding author at: College of Land Science and Technology, China Agricultural University, Beijing 100193, China.

E-mail address: yongchen@cau.edu.cn (Y. Chen).

¹ Xinlin Li and Lili Tan contributed equally to this paper.

the 21st century (Van Vuuren et al., 2011). Therefore, it is an indisputable fact that human activities have increased atmospheric CO₂ concentrations and amplified global warming (Stocker, 2014). The complexity and uncertainty of the future climate will affect the hydrological cycle, and thus alter the spatial and temporal distributions of regional water resources, which is closely related to the irrigation water availability and crop growth (Piao et al., 2010; IPCC, 2015).

Due to the negative impacts of climate change on agriculture, global food security has become one of the greatest challenges in the 21st century (McGuire, 2015). Changes in climatic conditions are expected to bring noticeable impacts on global food production (Teixeira et al., 2018). The increase in atmospheric CO₂ concentrations will induce the change in global temperature, rainfall pattern, and solar radiation, which are key factors that can influence crop productivity (Lobell et al., 2011). As an essential component for photosynthesis, the atmospheric CO₂ can directly affect crop growth and development and thus crop yield (Sreeharsha et al., 2015; Xu et al., 2016). Solar radiation is the energy source for crop growth, and an increase in solar radiation may mitigate the negative impacts by elevated air temperatures on crop yield. Study indicated that for every 1 MJ m⁻² increase in solar radiation, the yields for maize and wheat increased by 17.6 and 45.1 kg ha⁻¹, respectively (Xiao et al., 2020). Therefore, the interaction between climate change and crop growth is complex, and the evaluation of future climate change impacts on crop production is critical for global food security and sustainable production.

General Circulation Models (GCMs) are one of the primary tools for understanding future climate projections. Currently, the Coupled Model Intercomparison Project (CMIP) has entered its 6th phase (CMIP6), CMIP6 represents a greater expansion over CMIP5 and provides higher spatial resolution and improved physical parameters, which can support a larger amount of simulations. In addition, the key difference between CMIP5 and CMIP6 is the future scenarios. Compared to the Representative Concentration Pathways (RCPs) in CMIP5, CMIP6 uses a new set of emission scenarios, the Shared Socioeconomic Pathways (SSPs). The SSPs contain a series of projected future economic and social changes based on different socioeconomic assumptions. Some studies have revealed that CMIP6 models showed better simulation performance in predicting the future climate than CMIP5 models. For example, Hamed et al. (2022) compared two scenarios of CMIP5 (RCP4.5 and RCP8.5) with their CMIP6 counterparts (SSP2-4.5 and SSP5-8.5) in Egypt. The results showed that CMIP6 presented lower uncertainty in simulating seasonal air temperatures and rainfall changes than CMIP5. By comparing the CMIP5 and CMIP6 models in simulating daily precipitation periodicity of the global and regional scales, air temperature of the troposphere in East Asia, and long-term variation trends of surface air temperature in the Pacific Ocean, Wu et al. (2019) found that CMIP6 showed obvious improvements compared to CMIP5. Nevertheless, some studies also reported the CMIP6 GCMs displayed poorer performance than the CMIP5 GCMs. For instance, Zhu and Yang (2020) found that CMIP6 models exhibited lower simulation performance in simulating air temperature and precipitation in humid regions of the Tibetan Plateau compared to CMIP5 models. Song et al. (2021) simulated the changes in precipitation and air temperature in the middle and the end of the 21st century in South Korea under the RCP4.5 & RCP8.5 (CMIP5) and SSP2-4.5 & SSP5-8.5 (CMIP6) scenarios. The results showed that the SSP projections had higher uncertainty in simulating the precipitation, while the RCP projections showed higher uncertainty in terms of predicting air temperature. Therefore, it is necessary to evaluate the simulation performance of CMIP5 and CMIP6 GCMs at a specific regional scale first before using them for assessing the climate change impacts.

Commonly used hydrological models are the Soil and Water Assessment Tool (SWAT; watershed-scale model), the Agricultural Policy/Environmental eXtender (APEX; small watershed/field-scale model), the Variable Infiltration Capacity (VIC; a grid basis model), the McMaster University Hydrologiska Byrans Vattenbalansavdelning (MACHBV; rainfall-runoff model), etc. Among these, the physically-

based SWAT model is more suitable for a large watershed simulation with a high computation efficiency (Chen et al., 2018; Darbandsari and Coulibaly, 2020; Gassman et al., 2014; Kumari et al., 2021; Wang et al., 2020). In addition, unlike many hydrological models, SWAT is an open-source model (Arnold et al., 1998). In this study, an improved SWAT model with the management allowed depletion (MAD) auto-irrigation was used due to the source code is not restricted to the developers (Holzworth et al., 2015). The SWAT model can be coupled with GCMs to simulate dynamic changes in the hydrological cycle and crop growth, and thus analyze the spatial and temporal distributions of water resources and crop yields within a watershed. Using climate data from GCMs as input for the SWAT model is a common method to simulate the response of hydrological processes to climate change at the regional scale and has been widely used in various regions of the world (Marek et al., 2018; Chen et al., 2019; Tan et al., 2022).

The Daqing River Basin (DRB) in the North China Plain, which is densely populated and plays an important role in politics and the economy. At the same time, the basin is also a major national grain production region; however, the extreme shortage of water resources has become one of the critical factors limiting agricultural development (Jia et al., 2006). The winter wheat-summer maize rotation (double-cropping system) with intensive irrigation management is the main planting structure in the DRB (Zhang et al., 2022). The climate change on double-cropping system can have a significant effect on hydrological fluxes (Srivastava et al., 2020; Aghsaei et al., 2020; Tan et al., 2022). In the context of climate change, it is necessary to clarify the potential changes in irrigation water availability, actual evapotranspiration (ET_a), surface runoff, and crop production in the DRB for making better decisions on the management of soil and water resources to ensure the safety and reliability of food production. Therefore, the overall goal of this study is to more robustly assess the impacts of projected future climate change on the hydrological cycle and crop yields of winter wheat and summer maize in the DRB. The specific objectives of the study were to (1) screen out GCMs with high simulation accuracy from 10 groups of homologous GCMs of CMIP5 and CMIP6 using the Taylor Diagram method; (2) compare the key differences in the simulated hydrological cycle and crop growth in the study basin using an improved SWAT model driven by the selected homologous GCMs of CMIP5 and CMIP6; and (3) clarify the changing trends and reasons for the SWAT-MAD simulated hydrological components and crop yields in the study basin in future climate scenarios according to the final selection results of CMIPs and GCMs applicable to the study basin.

2. Materials and methods

2.1. Study area

The DRB lies between latitude 38°10'N-40°102'N and longitude 113°39'E-117°34'E, and its elevation varies between -16 to 2,687 m above mean sea level (Fig. 1). The total area of the basin is 43,060 km², of which 43.3% (18,659 km²) is a mountainous and hilly area, and 56.7% (24,401 km²) is plain and lowland area (Li et al., 2019). The DRB is located in the middle of the Haihe River Basin, which stretches approximately 275 km from east to west and approximately 200 km from north to south and runs through four provinces/cities, including Beijing, Tianjin, Hebei, and Shanxi. The study area has a semi-arid and semi-humid continental monsoon climate. The mean annual air temperature is 12.5°C; the mean annual air temperatures in the mountains and plains are 7.6°C and 13.1°C, respectively. The mean annual precipitation is approximately 500–600 mm, with great interannual variability. The annual sunshine hour ranges from 2,154 to 2,673 h. The major soil types are Mollic Gleysols, LITHOSOLS Eutic Cambisols, and Chromic Cambisols soils (Fig. 2). The predominant land use type in the study area is arable land, with approximately 48.94% coverage (Fig. 2), in which winter wheat and summer maize are the major crops.

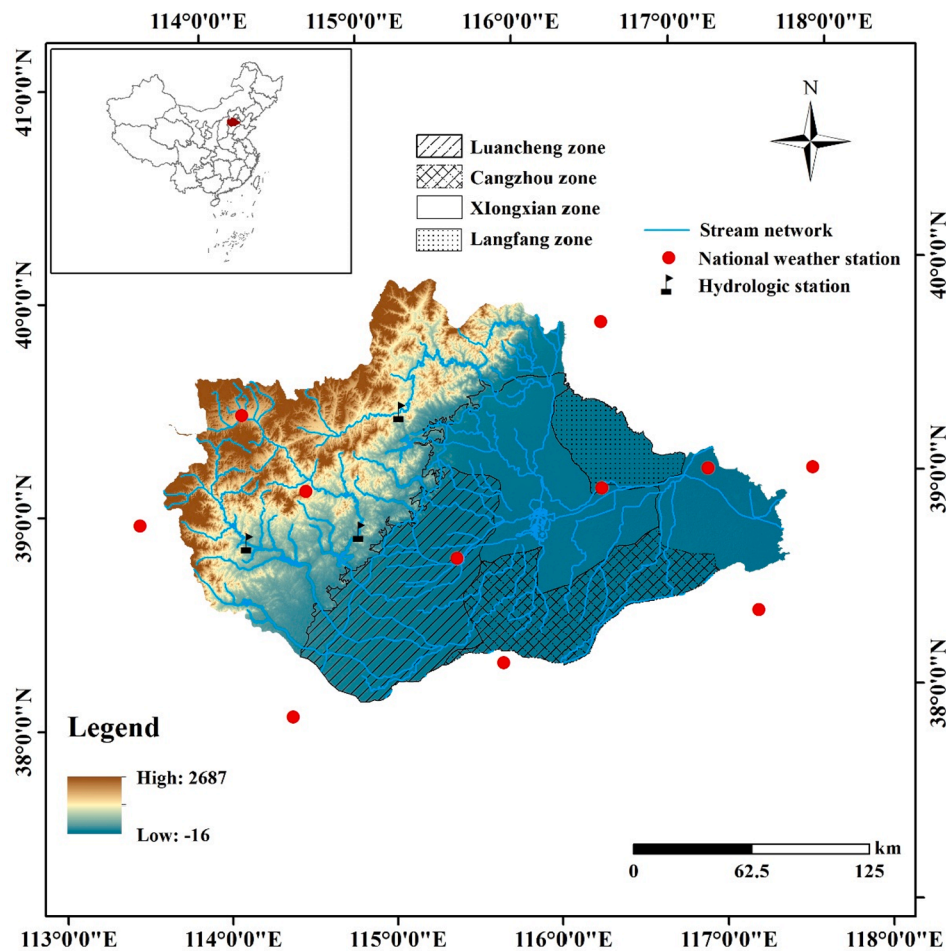


Fig. 1. Location of Daqing River Basin and distributions of weather and hydrological stations.

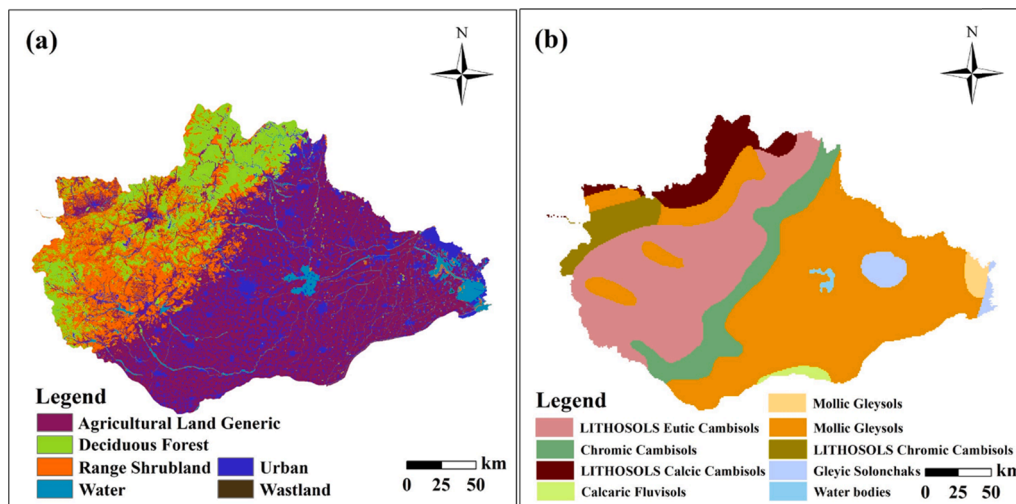


Fig. 2. Map of land uses (a) and soil types (b) in Daqing River Basin.

2.2. Future climate data of CMIP5 and CMIP6

2.2.1. Climate change scenarios

From 33 GCMs provided by the CMIP5 and 27 GCMs provided by the CMIP6, this study selected 10 groups of homologous GCMs from CMIP5 (RCP4.5 and RCP8.5 scenarios) and CMIP6 (SSP2-4.5 and SSP5-8.5 scenarios). The projected climate data were divided into two 30-year

periods: 2041–2070 and 2071–2100, using 1971–2000 as a historical period. The list of the GCMs used in this study and the description of different scenarios are shown in Table 1 and Table 2, respectively. Under the same emission scenario, CO₂ concentrations increased from 2041–2070 to 2071–2100. Over the same time period, the CO₂ concentrations elevated from 4.5 to 8.5 scenarios. The simulation performance of all GCMs was evaluated by integrating four climate factors,

Table 1

List of 10 pairs of GCMs from CMIP5 and CMIP6 used in this study.

Model ID	Institute ID	Country	CMIP5		CMIP6	
			GCM	Abbreviation	GCM	Abbreviation
01	CSIRO-BOM	Australia	ACCESS1.0	AC1	ACCESS-CM2	ACC1
02	CSIRO-BOM	Australia	ACCESS1.3	AC2	ACCESS-ESM1-5	ACC2
03	BCC	China	BCC-CSM1.1(m)	BC2	BCC-CSM2-MR	BCCC
04	CCCMA	Canada	CanESM2	CaE	CanESM5	CanI
05	EC-EARTH	Europe	EC-EARTH	ECE	EC-Earth3	ECE1
06	NOAA GFDL	USA	GFDL-CM3	GF2	GFDL-CM4	GFD2
07	INM	Russia	INM-CM4	INC	INM-CM4-8	INM1
08	IPSL	France	IPSL-CM5B-LR	IP3	IPSL-CM6A-LR	IPSL
09	MIROC	Japan	MIROC5	MI2	MIROC6	MIR1
10	MPI-M	Germany	MPI-ESM-LR	MP1	MPI-ESM1-2-LR	MPI2

Table 2

Scenario design and description.

Time period	Emission scenario		Radiative forcing	Change rate of radiative forcing	Assumed average CO ₂ concentration (ppm)*
	RCPs	SSPs	(W/m ⁻²)		
Historical (1971–2000)	—	—	—	—	330
2041–2070	RCP4.5	SSP2-4.5	4.5	Stabilizing	497
2071–2100	RCP4.5	SSP2-4.5	4.5	Stabilizing	533
2041–2070	RCP8.5	SSP5-8.5	8.5	Rising	578
2071–2100	RCP8.5	SSP5-8.5	8.5	Rising	807

* Meinshausen et al. (2011) and Van Vuuren et al. (2007).

mean annual precipitation, mean annual maximum air temperature (T_{max}), mean annual minimum air temperature (T_{min}), and mean annual solar radiation. The climate data from better performed GCMs were used as input data for an improved SWAT model to analyze the differences between CMIP5 and CMIP6 data in simulating the future changes in the hydrological cycle and crop growth. Furthermore, the CMIP (5 or 6) and GCMs with the best performance were chosen to evaluate the response of the hydrological cycle and crop growth to future climate change in the DRB.

2.2.2. Data processing for future climate

Daily weather data for the 1971–2000 period were obtained from 11 meteorological stations in the study basin, including T_{max} , T_{min} , precipitation (PCP), sunshine hours, relative humidity (HMD), and wind speed (WND). All the data were available at the Meteorological Data Center of the China Meteorological Bureau (CMA) (<https://data.cma.cn>). The daily solar radiation (SLR) within the study basin was calculated by using the Angstrom equation (Allen et al., 1998) from sunshine hours. Projected monthly weather data from 10 groups of GCMs were retrieved from the Coupled Model Intercomparison Project Phase 5 (CMIP5) (Taylor et al., 2012) and Phase 6 (CMIP6) (<https://esgf-node.llnl.gov/projects/cmip6>). RCP4.5, SSP2-4.5 (updated RCP4.5), RCP8.5, and SSP5-8.5 (updated RCP8.5) scenarios were selected in this study because they are more closely aligned with current socioeconomic development conditions. Under the moderate emission scenarios (RCP4.5 and SSP2-4.5), global CO₂ emissions are expected to peak around 2040 and then decline in the late 21st century; the atmospheric CO₂ concentrations will maintain stable at the end of the 21st century. RCP8.5 and SSP5-8.5 represent the high emission scenarios (Jones et al., 2013).

This study used a weather-generator based statistical (NWA1-WG) downscaling method developed by Liu and Zuo (2012) to transform the monthly climate data of 20 GCMs into daily data through spatial downscaling, deviation correction, and time downscaling. To reduce the uncertainty of the GCMs, this study used the projected climate data from GCMs developed by multiple countries (Liu et al., 2017) and the GCM projected outputs were changed using a second deviation correction, Equation 1 denoted the calculation method for the second deviation correction (Xiao et al., 2021). A 5-year warm-up period was adopted in

this study.

$$\Delta output_{var,GCM} = \frac{(S_{GCM} - S_{hist})}{S_{ob}} \times 100\% \quad (1)$$

where $\Delta output_{var,GCM}$ is the relative change; S_{GCM} , S_{hist} , and S_{ob} are SWAT simulated values driven by GCM projected climate for future period, GCM projected climate for historical period, and observed climate from weather stations, respectively.

2.2.3. Comparison and selection method of GCMs

The Taylor Diagram, proposed by Taylor in 2001, attracted wide attention of researchers because of its ability to effectively and intuitively demonstrate the performance difference of multiple models and the magnitude of errors between the simulated and actual values (Taylor, 2001). This study used the Taylor Diagram for the comparison and selection of GCMs. The basic principle involves three parameters, including the standard deviation, correlation coefficient, and root-mean-square error, which satisfy the cosine theorem relationship within the Taylor Diagram. Therefore, it is possible to identify the difference (indicating model accuracy) between the simulation values represented by scattering points on the Taylor Diagram and the actual values; on this basis, models can be compared and evaluated, and the models with the best performance will be selected. The calculation equations for the parameters are given as follows:

$$\sigma_r = \sqrt{\frac{1}{n} \sum_{i=1}^n (r_i - \bar{r})^2} \quad (2)$$

$$\sigma_f = \sqrt{\frac{1}{n} \sum_{i=1}^n (f_i - \bar{f})^2} \quad (3)$$

$$R = \frac{\sum_{i=1}^n (f_i - \bar{f})(r_i - \bar{r})}{\sigma_f \sigma_r} \quad (4)$$

$$NRMSE = \sqrt{\frac{1}{n} \sum_{i=1}^n [(f_i - \bar{f}) - (r_i - \bar{r})]^2} \quad (5)$$

$$S = \frac{4(1 + R)^2}{\left(\frac{\sigma_r}{\sigma_f} + \frac{\sigma_f}{\sigma_r}\right)^2 (1 + R_0)^2} \quad (6)$$

where n is the sample size; r is the observed value; f is the simulation value of the model; \bar{r} and \bar{f} are mean values of the observation data and simulation data, respectively; σ_r and σ_f are standard deviations of the observation data and simulation data, respectively; R is the correlation coefficient; R_0 is valued as 0.999; S is Taylor's skill score, and the larger S value indicates the better simulation performance of GCMs.

2.3. SWAT model

2.3.1. Overview of SWAT and SWAT-MAD

SWAT model can be used for simulating the hydrological cycle, pollution migration, and crop growth (Kim et al., 2020). In the SWAT model, the crop growth module uses a simplified version of the Environmental Policy Integrated Climate (EPIC) model to simulate crop yield based on the harvest index, potential biomass, water and temperature stress, etc. In the SWAT model, the agricultural management module provides the setting options for planting, harvest, fertilization, and irrigation based on the user requirements and actual conditions (Arnold et al., 1998).

The automatic irrigation algorithm in SWAT has some limitations. For example, the default automatic irrigation function of the soil water content method cannot reasonably simulate the irrigation demand of crops during a specific growth stage, which will also continue the irrigation in non-growing seasons and after harvest (Marek et al., 2017). In North China, with limited water resources, excessive irrigation will easily intensify the water resource shortage, and insufficient irrigation usually can result in a decrease in crop yield. For the aforementioned issues, Chen et al. (2018) developed a new set of auto-irrigation algorithms (management allowed depletion; MAD) by Fortran code in the SWAT model and completed a full testing and validation at the both field and watershed scales (Chen et al., 2018; Chen et al., 2020). Compared to the default automatic irrigation algorithm in SWAT, the improved MAD method has significantly improved the simulation of irrigation schedule with a relative deviation of 5% in the Texas High Plains, and has been widely used in the High Plains of Texas. The algorithm implements irrigation based on a water stress identifier of plant available water, in which MAD is the percentage of plant available water in soil and is usually set as 50%. When the soil water content is reduced to the user-defined MAD value, the irrigation will be triggered to recover soil water content according to the user-defined irrigation depth. This study used the "trial and error method" to determine the MAD thresholds of irrigation for winter wheat and summer maize, which were 0.3 and 0.4, respectively, and the irrigation depth was 25 mm for both crops (Tan et al., 2022).

2.3.2. SWAT model setup and data collection

This study is based on the SWAT model established by Tan et al. (2022), and the detailed SWAT model setup was initially reported in it. The required database and description of related data were listed in Table S1. The study basin includes 119 subbasins and 374 Hydrological Response Units (HRUs) according to the land use map (Fig. 2a), soil type map (Fig. 2b), and slope characteristics.

To better simulate agricultural conditions within the basin, this study divided the study basin into four zones (Fig. 1) based on the sowing and harvest time, irrigation regime, irrigation source, fertilization regime, and crop-growing parameters (Tan et al., 2022). Based on the collected data on four field experimental stations in Xiongxin, Luancheng, Langfang, and Nanpi in the plain area (Fig. 1) and the crop cultivation zone in Hebei Province, crop-growing parameters were calibrated and extended from field scale to regional scale after calibration. In this study, the agricultural management practices corresponding to the HRUs in the SWAT model in the plain area were established based on the data

collected from field experimental stations.

2.4. Calibration, validation, and evaluation of SWAT model

2.4.1. Calibration of model parameters and source of validation data

The monthly average streamflow at three hydrological stations (Zijingguan, Zhongtangmei, and Fuping stations) in the mountainous areas were used to calibrate related parameters, and aboveground biomass, LAI (leaf area index), and crop yield in plains and at field experimental stations were used to calibrate crop parameters of winter wheat and summer maize; the Surface Energy Balance System (SEBS) model, which was established based on the MODIS remote sensing data and observed daily climate data in the plain area of the DRB, was used to generate monthly actual evapotranspiration (ET_a) data from 2007 to 2016 to calibrate and validate the related parameters of the basin (Tan et al., 2022). Specifically, in the mountainous area of the DRB, this study calibrated the hydrological parameters with the monthly streamflow at three hydrological stations. The calibration period was 2010–2014, the validation period was 2015–2016, and the warm-up period was 1998–2009. In the plains, the ET_a from remote sensing data was used to calibrate SWAT parameters, with the warm-up period from 1998 to 2006, calibration period from 2007 to 2011, and validation period from 2012 to 2016. The periods for evaluating LAI, biomass, and crop yield of winter wheat and summer maize in the field experimental stations were 1999–2004, 2000–2014, and 1999–2016, respectively.

2.4.2. Evaluation of SWAT model

This study used nine performance indexes to evaluate the model, including the coefficient of determination (R^2), Nash-Sutcliffe coefficient (NSE), percentage bias ($PBIAS$), Willmott consistency index (d), mean error (ME), root-mean-square error ($RMSE$), normalized root-mean-square error ($NRMSE$), deviation of measured data (RSR), and Kling-Gupta coefficient (KGE). NSE is a normalized dimensionless statistical magnitude, which determines the relative size of residual variance and variance of measured data, with values ranging from $-\infty$ to 1. The larger the value is, the higher the simulation accuracy will be. Similar to NSE , the closer the KGE is to 1, the better the simulation performance will be. $PBIAS$ represents average variation trends of simulation data compared to the observed data. The closer the absolute value of $PBIAS$ is to 0, the better the simulation outcome will be. RSR varies from the optimal value 0 to ∞ , where 0 represents no residual variation. As a result, the lower the values of RSR and $RMSE$ are, the better the simulation performance of the model will be. d and $NRMSE$ are used for evaluating model accuracy in simulating crop growth variables. When d and $NRMSE$ are closer to 1 and 0, respectively, the simulation results are more accurate, in which the simulation results will be very good if $NRMSE < 10\%$; the simulation results are good if $NRMSE$ ranges between 10% and 20%; the simulation results are acceptable if $NRMSE$ ranges between 20% and 30%; and the simulation result are not acceptable if $NRMSE$ greater than 30% (Kumar et al., 2017; Mirsafi et al., 2016; Willmott, 1982; Gupta et al., 2009). The calculation equations were listed in Appendix A.

3. Results and discussion

3.1. Calibration and validation results of the SWAT model

The calibrated values of hydrological parameters in the study area were shown Table S2. The fitting curves of the simulated and observed values of streamflow during the calibration period (2010–2014) and validation period (2015–2016) for the Zijingguan, Zhongtangmei, and Fuping hydrological stations in the DRB are shown in Fig. S1. Overall, the simulated and observed values during the calibration and validation periods at three hydrological stations fitted well, in which the peak flows were well simulated. The values of R^2 and NSE at the Zijingguan, Zhongtangmei, and Fuping hydrological stations were larger than 0.7

and 0.6, respectively, during the calibration period (Table S3), which fulfilled the calibration requirement for streamflow (Li et al., 2016). The *PBIAS*, *RSR*, and *KGE* ranged from -4.4% to 10.9% , 0.34 to 0.53 , and 0.82 to 0.92 , respectively. During the validation period, values of R^2 and *NSE* at three hydrologic stations were greater than 0.87 and 0.75 , respectively, the *PBIAS* and *RSR* were -9.7% to -3.4% and 0.23 to 0.43 , respectively, and *KGE* was larger than 0.87 , which indicated the deviation between simulated and observed values was small. Overall, the simulated monthly streamflow during the calibration and validation periods well matched the observed data. During the calibration and validation periods, the *NRMSE* values of LAI, biomass, and yield for winter wheat and summer maize in experimental stations were smaller than 30% , with d greater than 0.67 and *RSR* < 1.64 , indicating a good simulation (Table S4). More detailed model performance results can also be found in Tan et al. (2022).

3.2. Direct comparison of the climate data between CMIP5 and CMIP6

By calculating the *S* value of annual precipitation, T_{\max} , T_{\min} , and solar radiation during the historical period (1971–2000), this study found that not all CMIP6 GCMs showed obvious improvement from their CMIP5 counterparts for future climate projections (Table 3). Compared with CMIP5 models, some CMIP6 GCMs showed poorer performance in simulating precipitation; for example, GFD2, IPSL, and MIR1. ACC1 and MIR1 models in CMIP6 performed worse in simulating the historical annual T_{\max} and T_{\min} than CMIP5 models. Similarly, GFD2, IPSL, and MIR1 models in CMIP6 showed poorer performance in simulating historical solar radiation than in CMIP5 models. Nevertheless, CMIP6 outperformed CMIP5 in simulating climate variables in the DRB. This study finally selected six CMIP5 GCMs and their corresponding updated versions in CMIP6 (six pairs of homologous GCMs from CMIP5 and CMIP6) (AC1-ACC1, BC2-BCCC, CaE-Can1, ECE-ECE1, GF2-GFD2, and MI2-MIR1), which showed reliable simulation results and an average score of *S* greater than 0.3 . This pre-selection could reduce the uncertainty caused by different GCMs in simulating future climate change.

Studies for directly comparing the simulation performance of CMIP5 and CMIP6 have been carried out worldwide. Zhu et al. (2020) found that CMIP6 GCMs had a stronger capacity for simulating historical precipitation in the arid area of the Tibet Plateau. Zhu et al. (2021) evaluated the simulation performance of CMIP5 and CMIP6 models for interannual precipitation characteristics in northern Africa, and the results also indicated that CMIP6 GCMs showed better simulation performance. However, some studies also indicated that CMIP6 GCMs had lower simulation performance compared to CMIP5 models. For instance, Song et al. (2021) compared the predicted changes in precipitation and temperature in South Korea based on the CMIP5 and CMIP6 GCMs under the future climate conditions. The projection results showed higher uncertainty under the CMIP6 SSP scenarios compared to the CMIP5 RCP scenarios (Song et al., 2021). Therefore, it is necessary to evaluate the performance of CMIP5 and CMIP6 GCMs at a regional scale first, and

then use the outperformed GCMs to drive the hydrological model for better assessing the climate change impacts on hydrology and crop growth.

3.3. Comparison of SWAT-MAD simulations driven by CMIP5 and CMIP6 GCM projections

For winter wheat.

Compared to the historical period, the precipitation during the winter wheat growing period simulated by six GCMs ranged from -2% to 45% and 5% to 41% under the RCP4.5 and SSP2-4.5 scenarios during the 2041–2070 period, respectively (Fig. 3a1,b1). Under the 2041–2070 RCP4.5 scenario, the ET_a during the winter wheat growing season increased from 1% to 5% (Fig. 3a4). The overall magnitude of increase in ET_a was greater under the SSP2-4.5 scenario than under the RCP4.5 scenario, and the average increase under both scenarios was approximately 3% . Studies have shown that LAI may increase gradually with increasing atmospheric CO_2 concentrations (Pritchard et al., 1999). Higher LAI indicates a larger contact area for photosynthesis, transpiration, and rainfall interception, resulting in the elevated transpiration and canopy evaporation and hence increase in ET_a (Phong et al., 2011). In addition, the increase in air temperature under future climate scenarios could enhance the transpiration of crops (Wang et al., 1995), which further led to the increase in annual irrigation for winter wheat. The increase in annual irrigation during the winter wheat growing period simulated by six GCMs under the 2041–2070 RCP4.5 scenario ranged from -4% to 11% (Fig. 3a2). Compared to the historical period, the annual average irrigation increased slightly under the 2041–2070 SSP2-4.5 scenario, but with a large variation among the models. Three GCMs predicted increasing trends in irrigation ranging from 1% to 6% ; whereas, the GCMs developed in China, Europe, and Japan projected decreasing trends in irrigation (Fig. 3b2). The surface runoff had a small change during the growing period of winter wheat under the RCP4.5 and SSP2-4.5 scenarios during the 2041–2070 period.

The projected precipitation showed similar trends under the RCP4.5 and SSP2-4.5 scenarios at the end of the 21st century (Fig. 3). The projected changes in annual precipitation, irrigation, surface runoff, and ET_a ranged from 5% to 41% , -4% to 11% , -0.2 to 2 mm, and 0.1% to 7% , respectively, under the RCP4.5 scenario at the end of the 21st century (Fig. 3a1,a2,a3,a4), and ranged from 11% to 44% , -4% to 8% , -1 to 2 mm, and 4% to 9% , respectively, under the SSP2-4.5 scenario (Fig. 3b1,b2,b3,b4). Under the RCP8.5 and SSP5-8.5 scenarios in the middle of the 21st century, the changes in annual precipitation, irrigation, surface runoff, and ET_a during the winter wheat growing period ranged from 6% to 39% & -6% to 34% , -1% to 8% & -7% to 6% , -0.4 mm to 1 mm & -1 mm to 3 mm, and -3% to 4% & -2% to 7% , respectively (Fig. 4). Compared to the historical period, the annual precipitation simulated by the six GCMs under the high emission scenarios showed increasing trends in the middle and end of the 21st century. Under the RCP8.5 and SSP5-8.5 scenarios, the magnitude of

Table 3
Evaluation scores for GCMs of CMIP5 and CMIP6.

CMIP5						CMIP6					
GCM	PCP	T_{\max}	T_{\min}	SLR	Ave. score	GCM	PCP	T_{\max}	T_{\min}	SLR	Ave. score
AC1	0.28	0.54	0.31	0.23	0.34	ACC1	0.41	0.28	0.30	0.47	0.37
AC2	0.22	0.39	0.23	0.26	0.28	ACC2	0.26	0.41	0.49	0.40	0.39
BC2	0.30	0.36	0.30	0.42	0.34	BCCC	0.46	0.52	0.39	0.53	0.47
CaE	0.15	0.23	0.54	0.42	0.34	Can1	0.33	0.44	0.49	0.43	0.42
ECE	0.27	0.26	0.37	0.45	0.34	ECE1	0.30	0.39	0.41	0.63	0.43
GF2	0.38	0.19	0.28	0.39	0.31	GFD2	0.22	0.17	0.49	0.37	0.31
INC	0.22	0.13	0.11	0.16	0.15	INM1	0.36	0.22	0.16	0.38	0.28
IP3	0.34	0.29	0.15	0.33	0.28	IPSL	0.25	0.31	0.44	0.22	0.31
MI2	0.42	0.35	0.48	0.51	0.44	MIR1	0.28	0.26	0.33	0.43	0.33
MP1	0.08	0.25	0.39	0.18	0.22	MPI2	0.31	0.42	0.43	0.28	0.36

Note: PCP, T_{\max} , T_{\min} , and SLR indicate precipitation, maximum air temperature, minimum air temperature, and solar radiation.

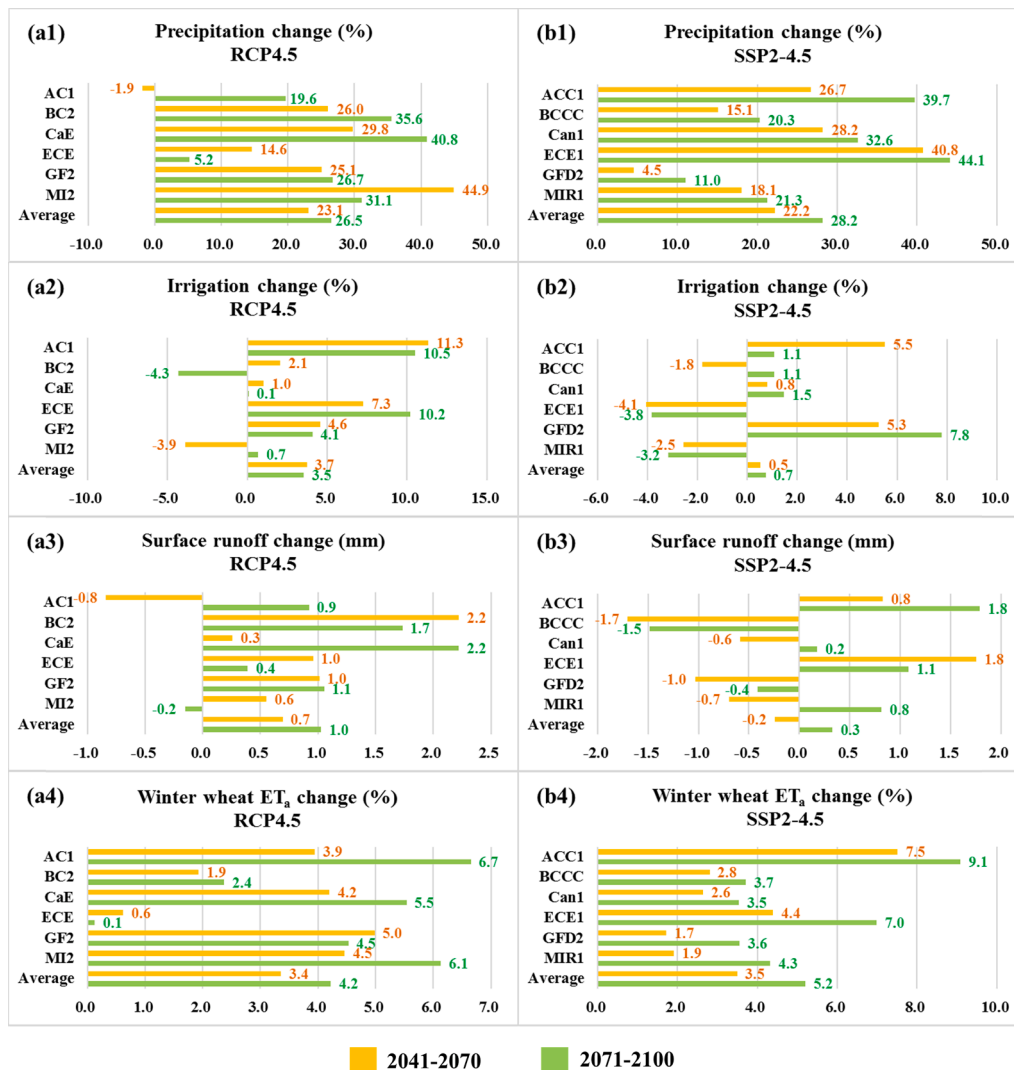


Fig. 3. Changes in annual precipitation, irrigation, surface runoff, and ET_a during the winter wheat growing period simulated by six GCMs under the RCP4.5 and SSP2-4.5 scenarios for the period of 2041–2070 and 2071–2100 compared to the historical period (1971–2000).

increases in precipitation was greater at the end of the 21st century ranging from 13% to 72% and 24% to 86%, respectively (Fig. 4a1,b1). Under the 2041–2070 RCP8.5 scenario, an overall increase in winter wheat irrigation was observed, with a range of –1% to 8% (Fig. 4a2). Under the 2041–2070 SSP5-8.5 scenario, the decreasing trends in irrigation were found, with an average decrease of 1% (Fig. 4b2).

The irrigation water demand decreased more prominently under the high emission scenarios at the end of the 21st century. Under the 2071–2100 RCP8.5 and 2071–2100 SSP5-8.5 scenarios, the projected decreases in annual irrigation during the winter wheat growing period ranged from 13% to 28% and 16% to 31%, respectively (Fig. 4a2,b2). Also, under the 2071–2100 RCP8.5 and 2071–2100 SSP5-8.5 scenarios, the changes in simulated ET_a ranged from –12% to –6% and –12% to –4%, respectively (Fig. 4a4,b4). The dramatically elevated atmospheric CO₂ concentration was the major reason for the decrease in ET_a (Kim et al., 2013). Studies have shown that high CO₂ concentrations might lead to partial closure in crop stomata and hence inhibit the transpiration of crop leaves (Wand et al., 1999; Medlyn et al., 2001). The future average surface runoff simulated by six GCMs under the above two scenarios at the end of the 21st century increased by 2 mm and 3 mm, respectively (Fig. 4a3,b3).

For summer maize.

The increases in precipitation during the summer maize growing

period under the moderate emission scenarios were greater at the end of the 21st century compared to the middle of 21st century (Figs. 9 and 10). Under the 2071–2100 RCP4.5 and 2071–2100 SSP2-4.5 scenarios, the changes in precipitation ranged from 14% to 53% and –8% to 67%, respectively (Fig. 5a1,b1). Under the 2041–2070 SSP2-4.5 scenario, the future precipitation predicted by the Can1 model decreased by 18% (Fig. 5b1). The changes in precipitation under the future climate scenarios could have direct impacts on the surface runoff for summer crop. Under the 2041–2070 RCP4.5 and 2041–2070 SSP2-4.5 scenarios, the changes in surface runoff were consistent with the trends of predicted precipitation. Under the 2041–2070 SSP2-4.5 scenario, in most GCMs, the simulated surface runoff increased with elevated precipitation, ranging from 3 mm to 111 mm (Fig. 5b3); except for the Can1 model, which predicted an 18 mm decrease in the surface runoff during the growing period of summer maize. Under the 2041–2070 RCP4.5 scenario, the simulated surface runoff increased from 1 mm to 31 mm. Overall, the percent increases in ET_a during the summer maize growing period were within 7% and 9% under the 2041–2070 RCP4.5 and 2041–2070 SSP2-4.5 scenarios, respectively (Fig. 5a4,b4). Some studies indicated that the increase in ET_a is mainly attributed to the increased LAI caused by rising CO₂ concentrations under future climate change (Phong et al., 2011; Wang et al., 1995; Shiru et al., 2021; Kim et al., 2013; Wand et al., 1999; Medlyn et al., 2001; Hickman et al., 2010).

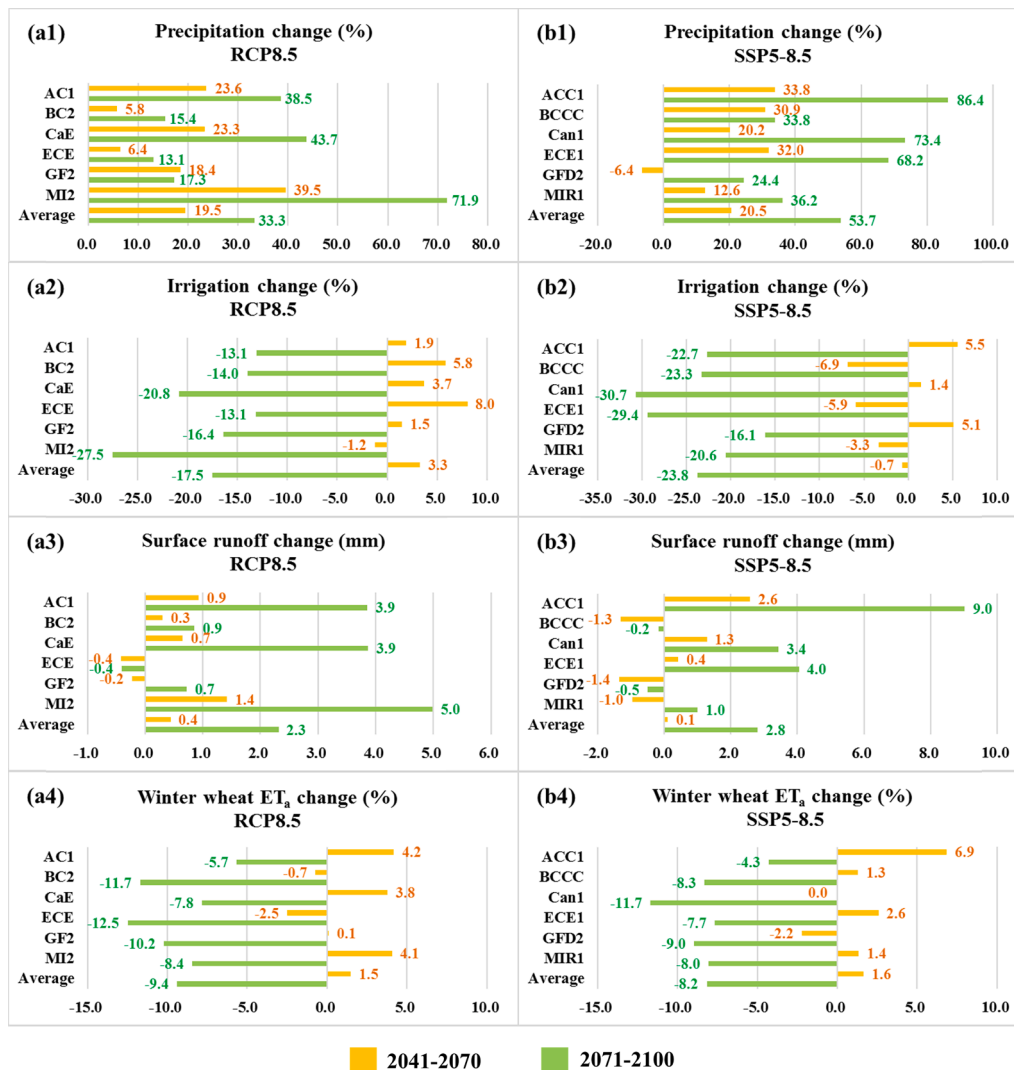


Fig. 4. Changes in annual precipitation, irrigation, surface runoff, and ET_a during the winter wheat growing period simulated by six GCMs under the RCP8.5 and SSP5-8.5 scenarios for the simulation period of 2041–2070 and 2071–2100 compared to the historical period (1971–2000).

Under the 2041–2070 RCP4.5 and 2041–2070 SSP2-4.5 scenarios, the irrigation showed decreasing trends ranging from -56% to -28% and -51% to 30%, respectively (Fig. 5a2,b2). The projected increases in precipitation in the study area might be sufficient to satisfy the higher demands on water for irrigation during the summer maize growing period.

By the end of the 21st century (2071–2100), the projected changes in irrigation, surface runoff, and ET_a for the RCP4.5 and SSP2-4.5 scenarios during the summer maize growing season were similar to the results simulated under the moderate emission scenarios for the period of 2041–2070, ranging from -80% to -36% & -55% to -23%, 10 mm to 50 mm & -8 mm to 95 mm, 4%-11% & 2%-11% (Fig. 5a2,b2,a3,b3,a4, b4). Under the 2041–2070 RCP8.5 and 2041–2070 SSP5-8.5 scenarios, the changes in annual precipitation during the summer maize growing period ranged from -3% to 45% and -5% to 48%, respectively. Under the 2041–2070 RCP8.5 and 2041–2070 SSP5-8.5 scenarios, only the ECE and Can1 models predicted decreases in precipitation (Fig. 6a1,b1). Under the 2041–2070 SSP5-8.5 scenario, the ET_a predicted by ECE1 and GF2 models decreased by 0.2% and 3%, respectively. However, the rest of the four GCMs projected increases in ET_a with a range from 1% to 7% (Fig. 6b4). Under the 2041–2070 RCP8.5 scenario, all six GCMs consistently predicted increases in the ET_a ranging from 1% to 7% (Fig. 6a4). Under the RCP8.5 and SSP5-8.5 scenarios for the middle of

the 21st century, increases in precipitation could have a direct impact on the increase of surface runoff. The average value of simulated surface runoff was larger under the SSP5-8.5 scenario than under the RCP8.5 scenario (Fig. 6a3,b3).

Under the high emission scenarios, the magnitude of increases in precipitation was larger at the end of the 21st century than in the middle of the 21st century. The surface runoff under the RCP8.5 and SSP5-8.5 scenarios at the end of the 21st century increased substantially, ranging from 25 mm to 90 mm and -5 mm to 132 mm, respectively (Fig. 6a3,b3). Due to the impacts of increased precipitation and CO₂ concentrations under the future climate, the irrigation water demand during the summer maize growing period under the RCP8.5 and SSP5-8.5 scenarios at the end of the 21st century decreased by 60%-88% and 41%-57%, respectively (Fig. 6a2,b2). Excessive CO₂ concentrations could reduce the irrigation water demand of summer maize by suppressing the leaf transpiration (Xiong et al., 2010), which further explained why the decrease in irrigation water demand was greater under the 2071–2100 RCP8.5 scenario than the rest three scenarios. The projected changes in ET_a during the growing period of summer maize varied greatly between different GCMs. Under the 2071–2100 RCP8.5 scenario, the increases in ET_a predicted by the AC1, CaE, and GF2 models were under 3%; whereas the other three GCMs projected decreases in ET_a ranging from -1% to -3% (Fig. 6a4). The simulation

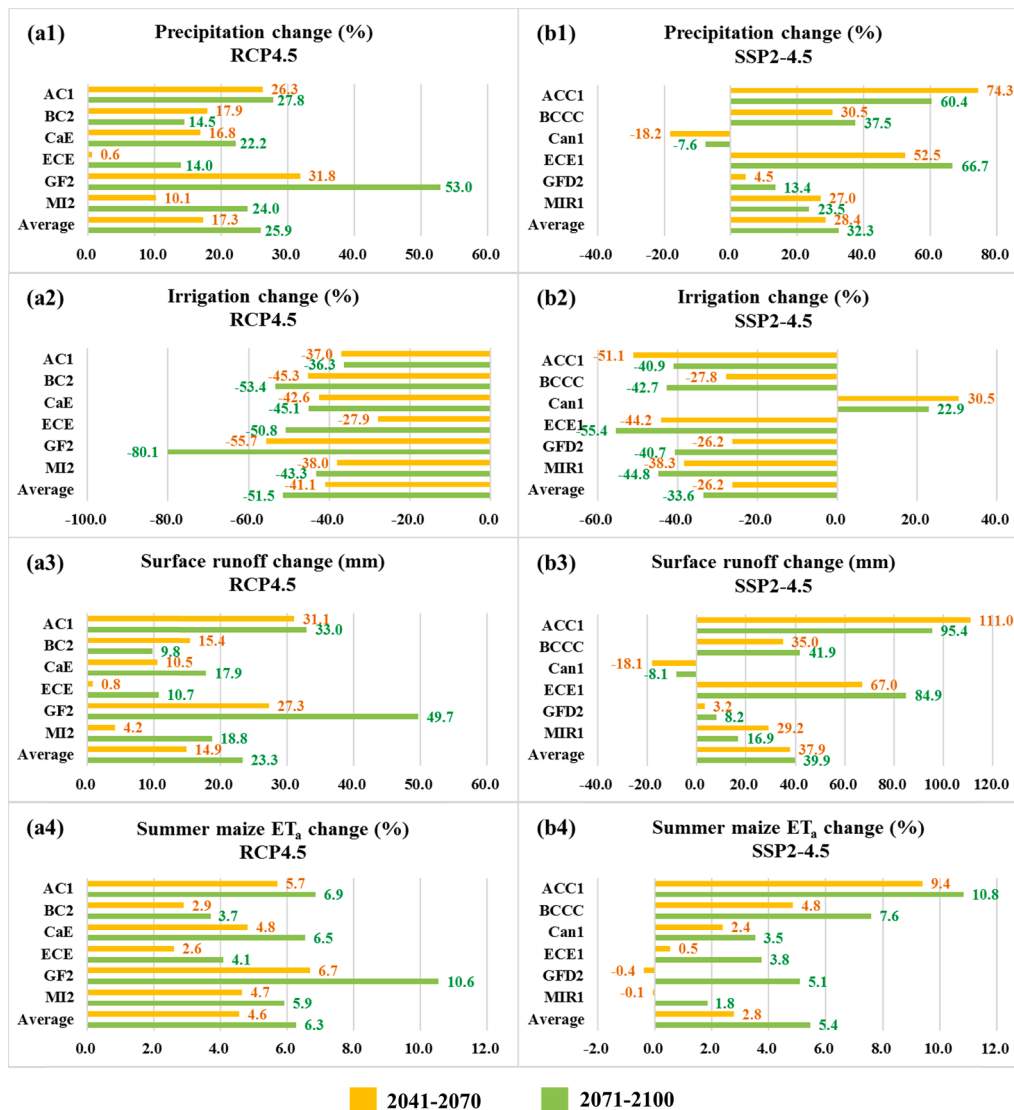


Fig. 5. Changes in annual precipitation, irrigation, surface runoff, and ET_a during the summer maize growing period simulated by six GCMs under the RCP4.5 and SSP2-4.5 scenarios for the period of 2041–2070 and 2071–2100 compared to the historical period (1971–2000).

results under the 2071–2100 SSP5-8.5 scenarios of CMIP6 were relatively consistent, with all models showing decreases in ET_a ranging from 1% to 10%, except for ACC1, which predicted a 7% increase in ET_a. The future ET_a of summer maize simulated by both CMIP5 and CMIP6 GCMs could decrease under the high emission scenarios at the end of the 21st century. Overall, the simulation results of the CMIP6 GCMs showed better stability and consistency than the CMIP5 model. Compared to the historical period, the changes in annual precipitation, irrigation, surface runoff, and ET_a of summer maize under the RCP8.5 and SSP5-8.5 scenarios at the end of 21st century ranged from 22% to 67% & –6% to 76%, –88% to 60% & –57% to –41%, 25 mm to 90 mm & –5 mm to 132 mm, and –1% to 3% & –10% to 7%, respectively (Fig. 6).

3.4. Comparisons of differences in simulating crop biomass, LAI, and yields using CMIP5 and CMIP6

Compared to the historical period, in the middle of the 21st century, the yield of winter wheat under the RCP4.5 and SSP2-4.5 scenarios increased by 16%–19% and 13%–25%, respectively. The average values of increases in yield simulated by six GCMs were 18% and 19%, respectively. The projected winter wheat yield under the RCP8.5 and SSP5-8.5 scenarios increased by 13%–23% and 14%–25%, respectively,

and the average values of increases in yield simulated by six GCMs were 16% and 19%, respectively. In the late 21st century, the yield of winter wheat under the RCP4.5 and SSP2-4.5 scenarios increased by 16%–20% and 13%–27%, respectively, and the average values of increases in yield simulated by six GCMs were 17% and 20% respectively. The simulated winter wheat yield under the RCP8.5 and SSP5-8.5 scenarios increased by 9%–20% and 6%–19%, respectively, and the average values of increases in yield simulated by six GCMs were 12% and 13%, respectively (Fig. 7). The magnitude of increases in winter wheat yield was slightly smaller under the high emission scenarios than the moderate emission scenarios. Dynamic curves of daily total biomass and LAI of winter wheat indicated similar trends under both CMIP5 and CMIP6 scenarios (Fig. 7a1,a2,a3,a4). The daily total biomass increased apparently under future climate change scenarios. The projected LAI of winter wheat increased in the early stage of growing period but declined in the late growing period compared to the historical period. Under future climate scenarios, the trend towards the earlier maturity of winter wheat would become more noticeable with higher CO₂ concentrations. This partially explained the magnitude of increase in yield was smaller under the high emission scenarios than in the moderate scenarios (Fig. 7).

Under the 2041–2070 RCP4.5 and 2041–2070 SSP2-4.5 scenarios, the yield of summer maize increased from 17% to 23% and 3% to 21%,

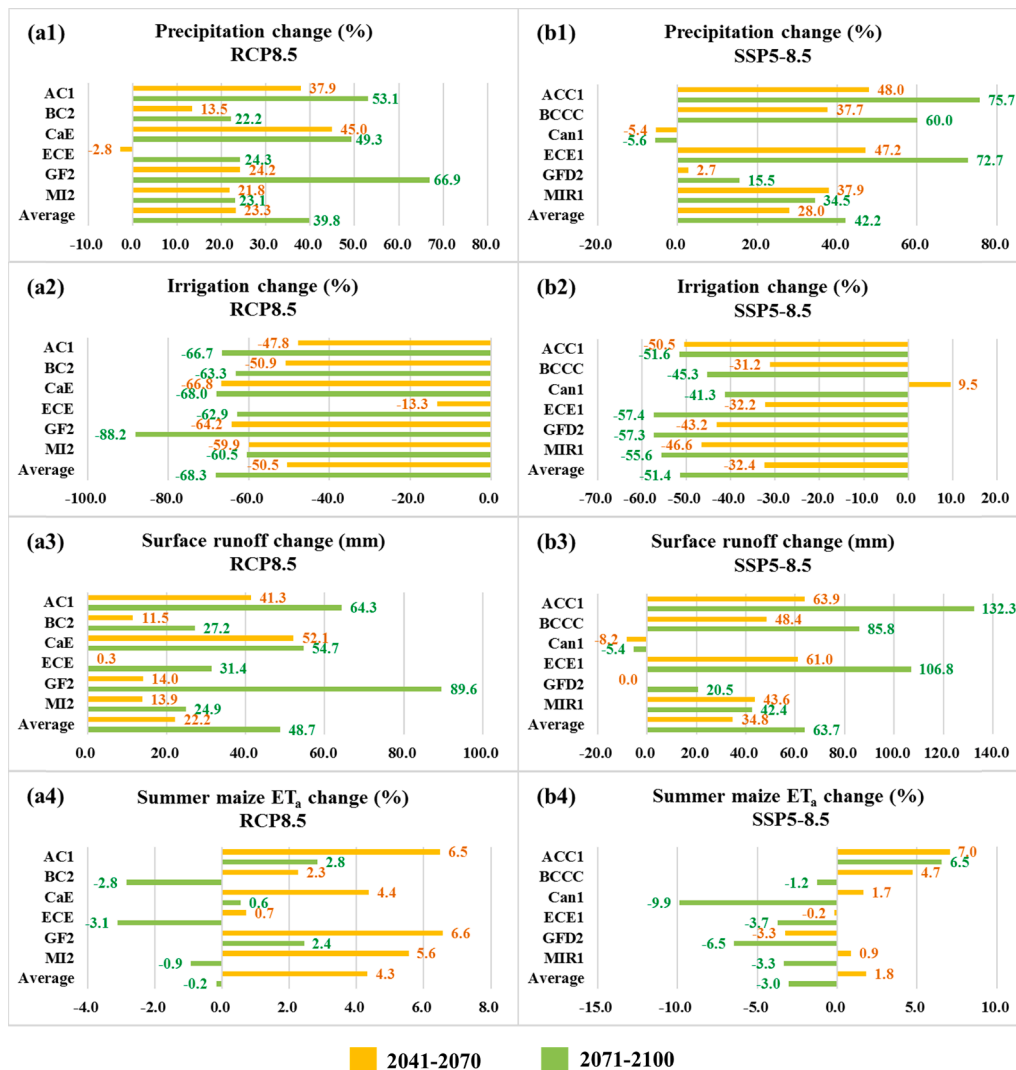


Fig. 6. Changes in annual precipitation, irrigation, surface runoff, and ET_a during the summer maize growing period simulated by six GCMs under the RCP8.5 and SSP5-8.5 scenarios for the periods of 2041–2070 and 2071–2100 compared to the historical period (1971–2000).

respectively, and the average values of increases in yield simulated by six GCMs were 20% and 12%, respectively, compared to the historical period. Under the 2071–2100 RCP4.5 and 2071–2100 SSP2-4.5 scenarios, the increases in summer maize yield ranged from 19% to 22% and 8% to 24%, respectively, and the average values of increases in yields simulated by six GCMs were 22% and 17% compared to the historical period, which were slightly higher than the scenarios in the middle of 21st century. The increase in atmospheric CO₂ concentrations might enhance the LAI and promote dry matter accumulation of plants and grain formation (Wang et al., 1998). Similar to the trends under the moderate emission scenarios, the summer maize yield also increased under the high emission scenarios due to the influence of increased CO₂ concentrations. Under the 2041–2070 RCP8.5, 2041–2070 SSP5-8.5, 2071–2100 RCP8.5, and 2071–2100 SSP5-8.5 scenarios, the increases in summer maize yield ranged from 18% to 24%, 7% to 23%, 17% to 34%, and 5% to 25%, respectively, and the average values of summer maize yield simulated by six GCMs increased by 21%, 15%, 24%, and 12%, respectively. In the middle and end of the 21st century, the magnitudes of increases in summer maize yields projected by the CMIP6 GCMs were slightly smaller than the CMIP5 GCMs (Fig. 7). Under the future climate scenarios, the increases in daily total biomass and LAI during the growing period of summer maize also indicated the tendency of early maturing and premature senility, which became more obvious

at the end of the 21st century, especially under the 2071–2100 SSP5-8.5 scenario (Fig. 7b1,b2,b3,b4). Generally, the direct comparison and the SWAT-MAD simulation results driven by GCMs of CMIP5 and 6 indicated better stability and consistency of CMIP6 compared to CMIP5. Therefore, the CMIP6 GCMs were further used for assessing the impacts of climate change on hydrologic and crop production in the DRB.

3.5. Response of hydrologic cycle and crop growth to future climate change based on the selected CMIP6 GCMs

3.5.1. Evaluation and selection of CMIP6 GCMs

Among 10 CMIP6 GCMs, most GCMs displayed good simulation performance and stability, but there were also some models with low performance scores (Fig. 8). For example, the GFD2 and IPSL achieved low scores in precipitation projections (Fig. 8a). The IPSL model was excluded from CMIP6 due to its worst accuracy in simulating solar radiation and lowest Taylor’s skill score (Fig. 8b). In terms of simulating the T_{max}, the GFD2 and INM1 models with the lowest scores were excluded from the study (Fig. 7). Regarding the projections of T_{min}, all GCMs in CMIP6 performed well with reasonable accuracy and stability, except the INM1 model, and hence INM1 model was excluded from the study. This study finally selected seven GCMs (ACC1, ACC2, BCCC, Can1, ECE1, MIR1, and MPI2) from 10 CMIP6 GCMs. The future climate

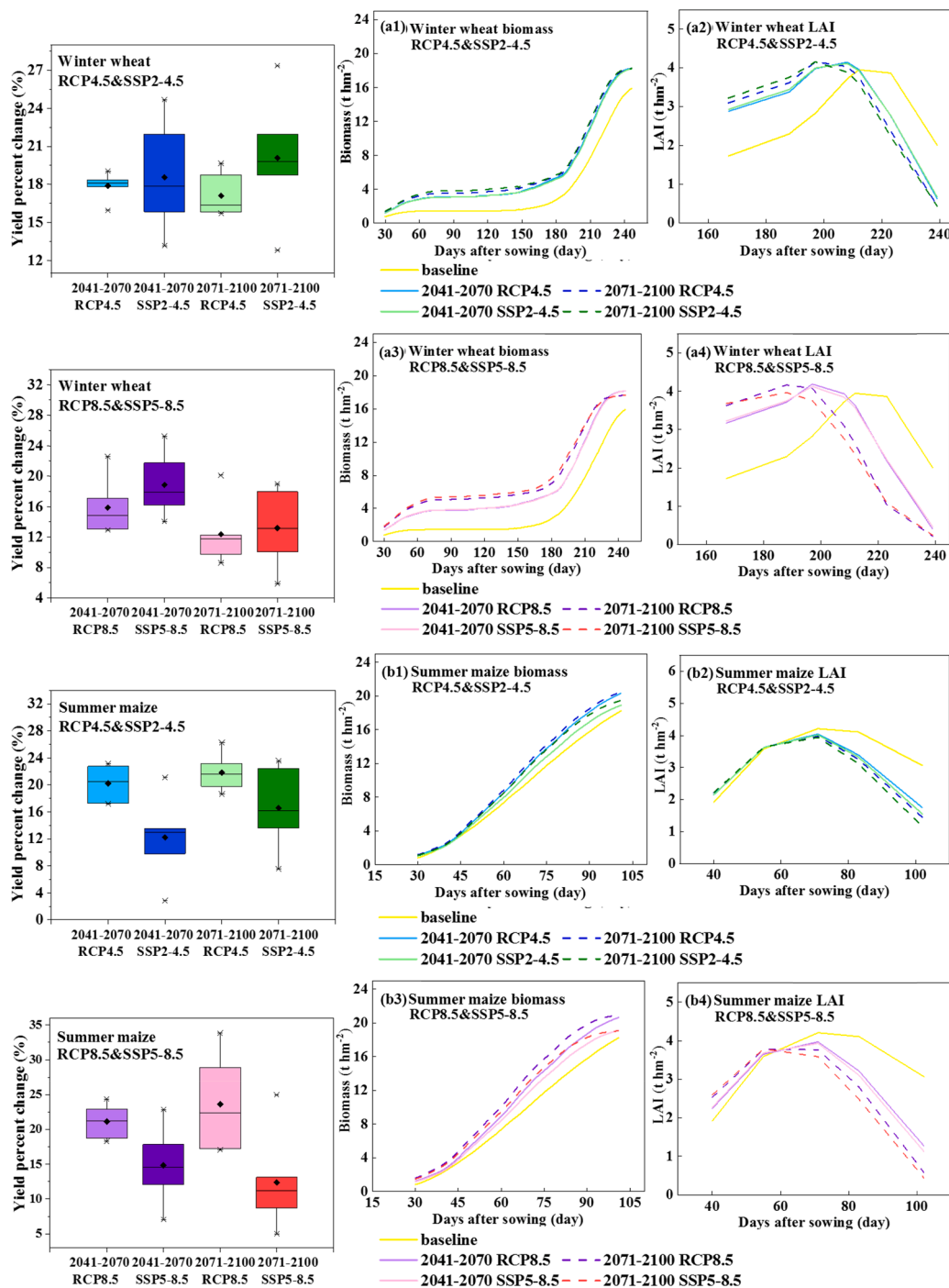


Fig. 7. Dynamic changes of daily total biomass, LAI, and yield during the growing season of crops under four scenarios (RCP4.5, SSP2-4.5, RCP8.5, and SSP5-8.5) for two simulation periods (2041–2070 and 2071–2100) relative to the historical period (1971–2000).

data projected by these GCMs were input into the SWAT-MAD model to analyze the changes in future climate, hydrologic cycle, and crop yields in the study watershed in the middle and at the end of the 21st century.

3.5.2. Characteristics of future climate change

Characteristics of future climate change during the growing period of winter wheat.

Compared to the historical period of GCMs, the increases in annual average T_{max} during the growing period of winter wheat in the plain area of the DRB ranged from 2.1°C to 4.2°C under the SSP2-4.5 and SSP5-8.5 scenarios for two simulation periods (2041–2070 and 2071–2100) (Table S5). The magnitude of increase in annual average

T_{max} was greater under the SSP5-8.5 scenario than the SSP2-4.5 scenario. Under the moderate emission scenarios, the annual average T_{max} increased by 2.1°C and 2.8°C in the middle and at the end of the 21st century, respectively. Under the high emission scenarios, the annual average T_{max} increased by 2.7°C and 4.2°C in the middle and at the end of the 21st century, respectively. The ranges of changes in T_{max} under the moderate emission scenarios and high emission scenarios were 1.4°C to 3.7°C and 1.8°C to 5.7°C, respectively (Table S5). Compared to the historical period of GCMs, GCMs developed in Australia projected higher increases in T_{max} , in which the T_{max} increased by 2.9°C and 3.7°C under the 2041–2070 SSP2-4.5 and 2071–2100 SSP2-4.5 scenarios, respectively. Germany’s MPI2 model projected a smaller increase in T_{max} in

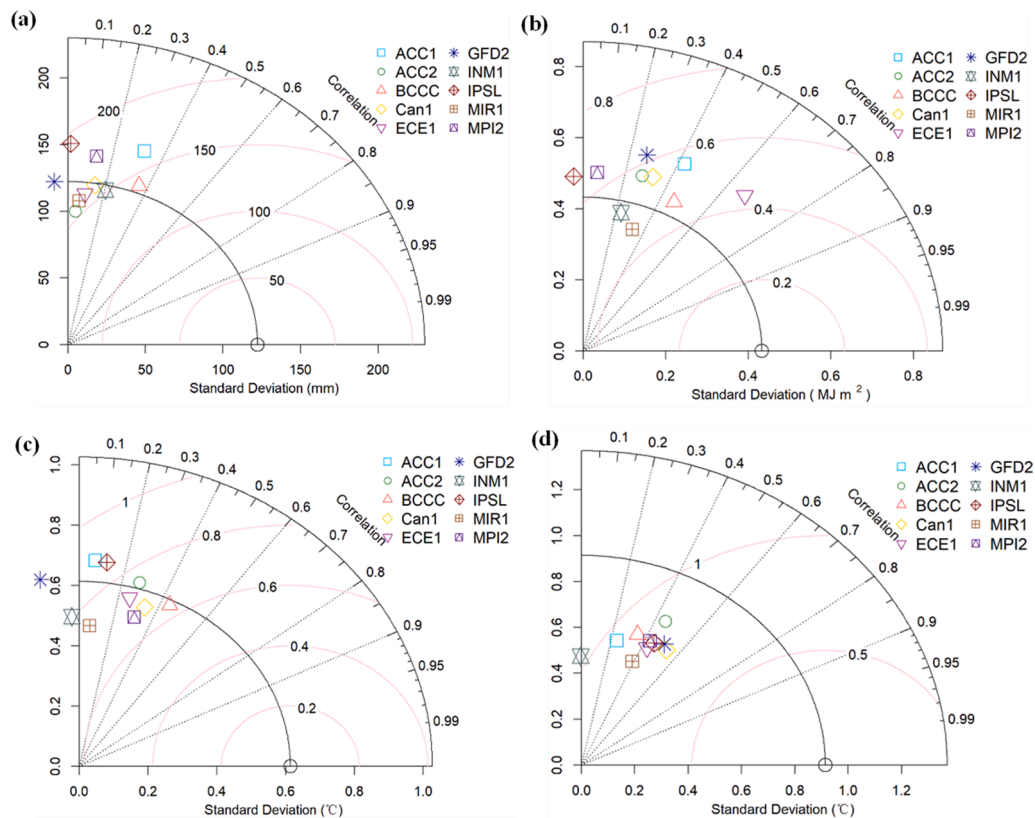


Fig. 8. Taylor Diagram of simulated precipitation (a), solar radiation (b), maximum air temperature (c), and minimum air temperature (d) for 10 GCMs of CMIP6.

which the T_{max} increased by 1.4°C, 2.0°C, 1.8°C, and 3.0°C under the 2041–2070 SSP2-4.5, 2071–2100 SSP2-4.5, 2041–2070 SSP5-8.5, and 2071–2100 SSP5-8.5 scenarios, respectively. The annual average T_{max} during the growing period of winter wheat simulated by China’s BCCC model increased by 1.8°C, 2.2°C, 2.0°C, and 3.1°C, respectively, under the 2041–2070 SSP2-4.5, 2071–2100 SSP2-4.5, 2041–2070 SSP5-8.5, and 2071–2100 SSP5-8.5 scenarios (Table S5).

According to the future climate data predicted by seven GCMs, the annual average T_{min} during the growing period of winter wheat in the plain area of the DRB increased by 2.4°C and 3.1°C under the 2041–2070 SSP2-4.5 and 2071–2100 SSP2-4.5 scenarios, respectively, compared to the historical period. The increases in annual average T_{min} were larger under the high emission scenarios. Specifically, annual average T_{min} increased by 3.1°C and 4.9°C under the 2041–2070 SSP5-8.5 and 2071–2100 SSP5-8.5 scenarios. The simulation results of annual

T_{min} during the winter wheat growing season varied greatly between the GCMs developed in different countries. For instance, the ranges of changes in annual T_{min} during the growing period of winter wheat were 1.1°C–4.6°C, 0.8°C–4.8°C, and 1.2°C–7.5°C under the 2041–2070 SSP5-8.5, 2071–2100 SSP2-4.5, and 2071–2100 SSP5-8.5 scenarios, respectively, compared to the historical period of GCMs. The predicted annual average T_{min} increased by 2.2°C, 2.7°C, 2.6°C, and 3.7°C under the 2041–2070 SSP2-4.5, 2071–2100 SSP2-4.5, 2041–2070 SSP5-8.5, and 2071–2100 SSP5-8.5 scenarios, respectively. The projection results of Australia’s ACC1 model were higher, and increases in annual T_{min} ranged from 3.8°C–4.6°C and 4.8°C–7.5°C in the middle and at the end of the 21st century, respectively. Canada’s Can1 model showed a lower prediction value, and the T_{min} increased by 0.6°C, 0.8°C, 1.1°C, and 1.2°C respectively under the 2041–2070 SSP2-4.5, 2071–2100 SSP2-4.5, 2041–2070 SSP5-8.5, and 2071–2100 SSP5-8.5 scenarios (Table S5).

Table 4

Relative changes in solar radiation during the growing period of crops in the plain area of the Daqing River Basin under the SSP2-4.5 and SSP5-8.5 scenarios in the middle and end of 21st century compared to the historical period (%).

GCM	2041–2070				2071–2100			
	SSP2-4.5		SSP5-8.5		SSP2-4.5		SSP5-8.5	
	winter wheat	summer maize						
ACC1	12.9	3.3	1.8	1.4	6.7	7.9	4.3	6.7
ACC2	31.8	3.1	0.6	3.4	0.6	7.5	−1.5	7.5
BCCC	15.8	1.3	−0.6	1.0	4.7	1.7	1.3	2.6
Can1	28.6	7.3	1.1	4.6	6.2	9.3	−3.1	−1.5
ECE1	13.6	−5.9	−4.7	−6.4	−0.3	−4.2	−6.4	−6.0
MIR1	−5.2	−5.1	−2.3	−4.5	−0.1	−2.5	−2.1	−2.0
MPI2	3.7	2.0	−1.5	3.4	0.7	5.8	−3.8	0.4
Maximum	31.8	7.3	1.8	4.6	6.7	9.3	4.3	7.5
Minimum	−5.2	−5.9	−4.7	−6.4	−0.3	−4.2	−6.4	−6.0
Average	14.5	0.8	−0.8	0.4	2.6	3.6	−1.6	1.1

In the middle and late 21st century, the annual average solar radiation increased by 14.5% and 2.6%, respectively, under the moderate emission scenarios, but decreased by 0.8% and 1.6%, respectively, under the high emission scenarios (Table 4). There were large differences among various models in predicting future solar radiation. Compared to the historical period, for instance, the ranges of changes in solar radiation under the 2041–2070 SSP2-4.5, 2071–2100 SSP2-4.5, 2041–2071 SSP5-8.5, and 2071–2100 SSP5-8.5 were −5.2% to 31.8%, −0.3% to 6.7%, −4.7% to 1.8%, and −6.4% to 4.3%, respectively.

Characteristics of climate change during the growing period of summer maize.

Compared to the historical period, for the periods of 2041–2070 and 2071–2100, the annual average T_{max} during the growing period of summer maize increased by 1.4°C and 1.9°C, respectively, under the moderate emission scenarios (Table S6). The annual average T_{max} in the middle and the end of the 21st century increased by 1.9°C and 3.0°C, respectively, under the high emission scenarios, with a range from 1.4°C to 2.4°C and 1.4°C to 4.4°C, respectively. The ACC1 model developed in Australia indicated the greatest increase in T_{max} under four scenarios compared to the rest of GCMs; the annual average T_{max} increased by 1.8°C, 2.6°C, 2.4°C, and 4.4°C, respectively, under the 2041–2070 SSP2-4.5, 2071–2100 SSP2-4.5, 2041–2070 SSP5-8.5, and 2071–2100 SSP5-8.5 scenarios. The ECE1 model developed in Europe showed the lowest increase in T_{max} under the SSP2-4.5 scenario compared to the rest of GCMs; under the 2041–2070 SSP2-4.5 and 2071–2100 SSP2-4.5 scenarios, the annual average T_{max} increased by 0.9°C and 1.2°C, respectively. The T_{max} projected by the BCCC model developed in China increased by 1.6°C, 1.8°C, and 3.4°C under the 2041–2070 SSP2-4.5, 2071–2100 SSP2-4.5, and 2071–2100 SSP5-8.5 scenarios, respectively.

Four emission scenarios indicated that the annual average T_{min} during the growing period of summer maize in the plain area of the DRB increased, but the magnitude of increases projected varied due to model differences (Table S6). In the middle of the 21st century, the annual T_{min} during the growing period of summer maize among seven GCMs increased from 1.3°C to 4.0°C and 1.9°C to 4.9°C under the SSP2-4.5 and the SSP5-8.5 scenarios, respectively. By the end of the 21st century, the annual T_{min} during the growing period of summer maize among seven GCMs increased from 1.4°C to 5.3°C and 1.3°C to 8.1°C under the SSP2-4.5 and SSP5-8.5 scenarios, respectively (Table S6). Compared to the historical period of GCMs, the annual average T_{min} during the growing period of summer maize increased by 2.7°C, 3.4°C, 3.5°C, and 5.3°C under the 2041–2070 SSP2-4.5, 2071–2100 SSP2-4.5, 2041–2070 SSP5-8.5, and 2071–2100 SSP5-8.5 scenarios, respectively. The projected values of Can1 model developed in Canada were maintained at a low level. Simulations results from two models developed in Australia were greater, in which the projection values of ACC1 model were highest under all scenarios compared to the rest six GCMs; specifically, the annual average T_{min} during the growing period of summer maize increased by 4.0°C, 5.3°C, 4.9°C, and 8.1°C, respectively under the 2041–2070 SSP2-4.5, 2071–2100 SSP2-4.5, 2041–2070 SSP5-8.5, and 2071–2100 SSP5-8.5 scenarios.

Compared to the historical period, solar radiation during the summer maize growing period increased by 0.8%, 3.6%, 0.4%, and 1.1% under the 2041–2070 SSP2-4.5, 2071–2100 SSP2-4.5, 2041–2070 SSP5-8.5, and 2071–2100 SSP5-8.5 scenarios, respectively. Among all GCMs, the ECE1 model developed in Europe had the lowest simulation results; in the middle and the end of the 21st century, the annual average solar radiation decreased by 5.9% and 4.2%, respectively, under the moderate emission scenarios, and 6.4% and 6.0%, respectively, under the high emission scenarios. The Can1 model developed in Canada showed the highest increases in annual solar radiation under the 2041–2070 SSP2-4.5, 2071–2100 SSP2-4.5, and 2041–2070 SSP5-8.5 scenarios, which were 7.3%, 9.3%, and 4.6%, respectively (Table 4). Xiao et al. (2020) predicted increases in solar radiation from 2040 to 2080 in the North China region based on 33 GCMs under two RCPs (RCP4.5 & RCP8.5) scenarios.

3.5.3. Effects of future climate change on the hydrological cycle and crop yields

Changes in the hydrological cycle and crop yield during the growing period of winter wheat.

Under the future climate scenarios, the ranges of changes in annual precipitation, irrigation, ET_a , surface runoff, and yield of winter wheat projected by seven GCMs were 22.9% to 57.6%, −24.6% to −0.5%, −7.9% to 5.2%, −0.2 mm to 4.1 mm, and 11.4% to 18.9%, respectively, compared to the historical period (Table 5). In the middle and end of the 21st century, the simulated annual average precipitation increased in various degrees under the SSP2-4.5 and SSP5-8.5 scenarios compared to the historical period. Under the SSP2-4.5 and SSP5-8.5 scenarios, the increases in precipitation in the late 21st century were greater than the middle of the 21st century. Future increases in precipitation could lead to a decrease in irrigation to a certain extent. In addition, the apparent increases in precipitation and atmospheric CO_2 concentration under the 2071–2100 SSP5-8.5 scenario might lead to a decrease in ET_a during the growing period of winter wheat and a substantial increase in annual average surface runoff, which could result in lower irrigation relative to the historical period and the other three climate change scenarios. The increase in CO_2 concentrations might lead to the decrease of crop stomatal conductance and restrain the transpiration, which could further reduce the ET_a . However, the increase in LAI due to the elevated CO_2 concentrations could provide a larger surface area for transpiration, rainfall interception, and photosynthesis, which might result in increases in ET_a during the growing period of winter wheat under the moderate emission scenarios and the 2041–2070 SSP5-8.5 scenario (Hickman et al., 2010). The temperature and water stress days were projected to decrease under all emission scenarios compared to the historical period. By the late 21st century, the trend towards fewer temperature and water stress days would become more prominent, particularly under the scenario of SSP5-8.5 (Fig. 9).

As a C_3 crop, winter wheat can benefit from the increase in CO_2 concentrations (Deryng et al., 2016; Cotterman et al., 2018). The projected increases in winter wheat yield were attributed to the sufficient supply of CO_2 and the decrease in temperature and water stress days. Moreover, autumn sowing and summer harvesting of the winter wheat could avoid the impact of the extremely hot and dry climate in the summer of the North China Plain. In this study, the simulated solar radiation during the growing period of winter wheat increased under the moderate emission scenarios and decreased noticeably under the high emission scenario at the end of 21st century (Table 4). Many studies indicated that solar radiation might have a direct influence on crop yield. For example, Zhang et al. (2013) observed a positive correlation between the wheat yield and solar radiation through field experiments. Xiao and Tao (2014) used a wheat module in APSIM (Agricultural Production Systems sIMulator) to simulate the impacts of climate

Table 5

Simulated annual average irrigation (mm), ET_a (mm), surface runoff (mm), and yield ($kg\ ha^{-1}$) during the growing period of winter wheat under the future emission scenarios compared to the historical period (1971–2000).

Scenario	Precipitation	Irrigation	ET_a	Surface runoff	Crop yield
1971–2000	112.8	222.5	376.3	2.5	5498.5
2041–2070	141.5 (24.8)	220.3	391.0	2.3 [−0.2]	6468.3
SSP2-4.5		(−0.9)	(3.7)		(17.6)
2071–2100	150.3 (32.5)	221.3	396.9	3.0 [0.5]	6535.1
SSP2-4.5		(−0.5)	(5.2)		(18.9)
2041–2070	139.2 (22.9)	220.8	384.9	2.9 [0.4]	6522.2
SSP5-8.5		(−0.7)	(2.2)		(18.6)
2071–2100	179.3 (57.6)	162.5	345.3	6.6 [4.1]	6123.7
SSP5-8.5		(−24.6)	(−7.9)		(11.4)

Note: The numbers in () are the percent changes in climate variables under the emission scenarios relative to the historical period; the numbers in [] are the absolute changes in climate variables under the emission scenarios relative to the historical period.

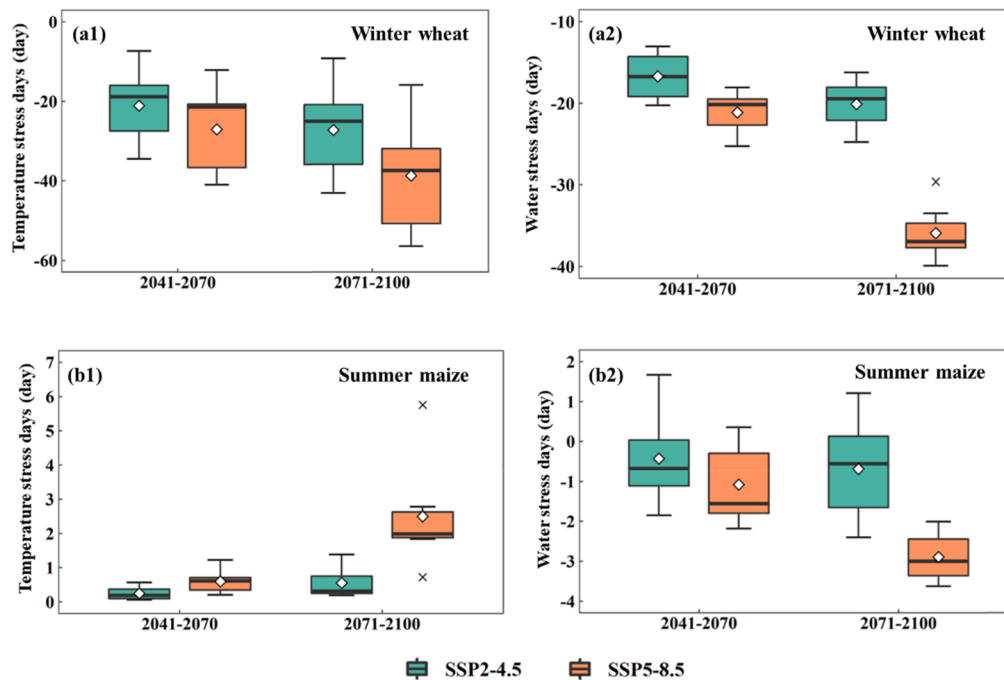


Fig. 9. Changes in annual average temperature stress days and water stress days simulated by 7 GCMs during the growing period of crops under the SSP2-4.5 and SSP5-8.5 scenarios for the periods of 2041–2070 and 2071–2100 compared to the historical period (1971–2000).

variables on wheat yields at four sites from 1980 to 2009. The study found that the wheat yields declined by 3.0%–12.0% due to the substantial decrease in solar radiation over the past four decades.

Results in this study also indicated a lower increase in winter wheat yield under 2071–2100 SSP5-8.5 scenarios compared to other scenarios. However, a substantial increase in CO₂ concentrations and a decrease in temperature and water stress days can offset the negative effects of a slightly decreased solar radiation (Tao et al., 2008; Zhang, 2012), which finally led to an overall increase in yield. Under the condition of sufficient irrigation water supply, therefore, the yields of winter wheat might increase steadily under the SSP2-4.5 and SSP5-8.5 scenarios in the middle and the end of the 21st century due to the combined effects of increased CO₂ concentrations, air temperatures, precipitation, and fluctuation of solar radiation.

Variations in the hydrological cycle and crop yield during the growing period of summer maize.

Compared to the historical period, the ranges of changes in annual precipitation, irrigation, ET_a, surface runoff, and yield of summer maize simulated by seven GCMs were 29.4% to 46.6%, –48.9% to –22.7%,

Table 6

Simulated annual average irrigation (mm), ET_a (mm), surface runoff (mm), and yield (kg ha⁻¹) during the growing period of summer maize under the future emission scenarios compared to the historical period (1971–2000).

Scenario	Precipitation	Irrigation	ET _a	Surface runoff	Crop yield
1971–2000	387.9	34.8	301.4	33.1	6058.3
2041–2070	502.3 (30.1)	21.9	313.4	72.9	6867.7
SSP2-4.5		(–22.7)	(3.8)	[39.9]	(13.3)
2071–2100	511.9 (32.6)	18.3	320.9	73.8	7073.2
SSP2-4.5		(–29.1)	(6.2)	[40.7]	(16.7)
2041–2070	499.7 (29.4)	18.7	311.1	69.6	7021.5
SSP5-8.5		(–28.5)	(3.1)	[36.5]	(15.8)
2071–2100	565.1 (46.6)	7.1 (–48.9)	295.8	101.2	6840.2
SSP5-8.5			(–1.8)	[68.1]	(12.9)

Note: The numbers in () are the percent changes in climate variables under the emission scenarios relative to the historical period; the numbers in [] are the absolute changes in climate variables under the emission scenarios relative to the historical period.

–1.8% to 6.2%, 36.5 mm to 68.1 mm, and 12.9% to 16.7%, respectively (Table 6). The increase in future precipitation was the main factor that led to the decrease in irrigation and increase in surface runoff. Under the moderate emission scenarios and the 2041–2070 SSP5-8.5 scenario, the ET_a during the growing period of summer maize increased slightly, which was attributed to the projected increases in precipitation and LAI during the summer maize growing season (Wu and Liu, 2012). By the end of 21st century, under the high emission scenarios, when the projected CO₂ concentration reached 807 ppm, the crop stomata could close partially and transpiration could be restrained significantly, resulting in a decrease in ET_a and thus a decrease in water demand for irrigation during the growing period of summer maize (Jonathan et al., 2014; Wu et al., 2012). Overall, the temperature stress days during the growing period of summer maize increased slightly, while the water stress days decreased slightly (Fig. 9).

The increase in air temperatures and temperature stress days in the future can accelerate the early maturing of crops and reduce the growth time of summer maize. However, the increase in CO₂ concentration, solar radiation, precipitation, decrease in water stress days, and sufficient irrigation water supply would fully satisfy crop growth needs. Therefore, future climate change could eventually have a positive effect on the biomass accumulation and yield of summer maize.

4. Conclusions and limitations

Out of 33 GCMs from CMIP5 and 27 GCMs from CMIP6, 10 pairs of homogeneous GCMs were selected in this study. After analyzing the annual precipitation, maximum and minimum air temperatures, and solar radiation, six pairs of GCMs of CMIP5 and CMIP6 with better simulation performance were screened out. The future climate data from the six pairs of GCMs were used as input for the SWAT-MAD model to analyze the changes in hydrological cycle and crop growth during the growing periods in the DRB under moderate and high emission scenarios for the periods of 2041–2070 and 2071–2100. The results showed that the annual average precipitation could increase under four scenarios in the middle and the end of the 21st century, and the increases of annual average precipitation were greater under the CMIP6 SSP scenarios than

the CMIP5 RCP scenarios; the maximum percentage increases of precipitation during the growing periods of winter wheat and summer maize were 54% and 42%, respectively. By the end of the 21st century, the projected changes in hydrological cycle were similar under the high emission scenarios of CMIP5 and CMIP6; the decrease in ET_a and substantial increase in precipitation during the crop growing periods could lead to a decrease in irrigation and a clear increase in surface runoff. Under the RCP4.5 & SSP2-4.5 and RCP8.5 & SSP5-8.5 scenarios in the middle and the end of the 21st century, the dynamic changes in daily biomass and LAI of winter wheat and summer maize in the growing period showed similar trends for CMIP5 and CMIP6. In addition, the future daily biomass and LAI of winter wheat and summer maize were projected to increase in the early growth period with a tendency of early maturing and premature senescence. The increases in crop yields of winter wheat and summer maize were greater under the moderate scenarios than the high emission scenarios due to the reductions in solar radiation under the high emission scenarios.

Overall, the comparisons of GCMs between CMIP5 and CMIP6 emphasized the higher stability and consistency of CMIP6 than CMIP5. Furthermore, seven GCMs with better simulation performance were further selected from CMIP6 based on the Taylor Diagram for more accurately evaluating the climate change impacts in the DRB. The annual average precipitation and air temperatures were increased clearly for both the winter wheat and summer maize growing periods under the future climate change scenarios. However, the annual average solar radiation during the growing period of winter wheat in the middle and the end of the 21st century increased by 14.5% and 2.6%, respectively, under the moderate emission scenarios, and decreased by 0.8% and 1.6% under the high emission scenarios, respectively. Under the future climate scenarios, the changes in irrigation, ET_a , and surface runoff during the winter wheat growing period projected by seven GCMs ranged from -24.6% to -0.5%, -7.9% to 5.2%, and -0.2 mm to 4.1 mm, respectively, compared to the historical period. Those values for summer maize varied from -48.9% to -22.7%, -1.8% to 6.2%, and 36.5 mm to 68.1 mm. Under the conditions of sufficient water supply for irrigation, the yields of winter wheat and summer maize in the DRB increased steadily under the SSP2-4.5 and SSP5-8.5 scenarios in the middle and the end of the 21st century due to the combined effect of CO_2 concentration, solar radiation, precipitation, and air temperatures. Compared to the historical period, the maximum increases in yields of winter wheat and summer maize were 18.9% and 16.7%, respectively. The findings in this study for future climate change and their impacts on hydrology and crop production using CMIP5 and CMIP6 can provide technical support for the pre-selection of CMIPs and GCMs for other climate change studies and offer decision-making support for agricultural best management strategies at a basin level.

Although the spatial variations in soil, land use, and agricultural management inputs have been sufficiently considered in this study, the SWAT model itself still has some uncertainties inevitably, including

input data and parameter adjustments, and so on. In this study, Taylor's method was used to select the outperformed CMIPs and GCMs. However, due to the complexity of climate change issues and the limitations of human cognition, the projected changes in future climate showed a high variation among different CMIPs and GCMs. In addition, there were many causes of uncertainties in climate projections, e.g., downscaling approaches, bias-correction methods, etc.

CRediT authorship contribution statement

Xinlin Li: Conceptualization, Funding acquisition, Software, Validation, Formal analysis, Investigation, Writing – original draft, Writing – review & editing, Visualization. **Lili Tan:** Conceptualization, Funding acquisition, Software, Validation, Formal analysis, Investigation, Resources, Writing – review & editing, Visualization. **Yingxuan Li:** Writing – review & editing. **Junyu Qi:** Writing – review & editing. **Puyu Feng:** Writing – review & editing. **Baoguo Li:** Writing – review & editing, Supervision, Project administration. **De Li Liu:** Writing – review & editing. **Xueliang Zhang:** Writing – review & editing. **Gray W. Marek:** Writing – review & editing. **Yingqi Zhang:** Writing – review & editing. **Haipeng Liu:** Writing – review & editing. **Raghavan Srinivasan:** Writing – review & editing. **Yong Chen:** Conceptualization, Funding acquisition, Software, Validation, Formal analysis, Investigation, Resources, Writing – original draft, Writing – review & editing, Supervision, Project administration.

Declaration of Competing Interest

The authors declare that they have no known competing financial interests or personal relationships that could have appeared to influence the work reported in this paper.

Data availability

Data will be made available on request.

Acknowledgements

This research was supported by the Chinese Universities Scientific Fund under award numbers 1191-15051002, 1191-31051204, 1191-10092004, and 1191-15052008. The research was also partially supported by the National Institute of Food and Agriculture, U.S. Department of Agriculture under award number NIFA-2021-67019-33684. This research was supported in part by the Ogallala Aquifer Program, a consortium between USDA-Agricultural Research Service, Kansas State University, Texas A&M AgriLife Research, Texas A&M AgriLife Extension Service, Texas Tech University, and West Texas A&M University. We appreciate anonymous reviewers for their valuable comments and suggestions.

Appendix A

$$R^2 = \frac{[\sum_i (Q_{m,i} - \bar{Q}_m)(Q_{s,i} - \bar{Q}_s)]^2}{\sum_i (Q_{m,i} - \bar{Q}_m)^2 \sum_i (Q_{s,i} - \bar{Q}_s)^2} \quad (1)$$

$$NSE = 1 - \frac{\sum_i (Q_{s,i} - Q_{m,i})^2}{\sum_i (Q_{m,i} - \bar{Q}_m)^2} \quad (2)$$

$$PBIAS = \frac{\sum_{i=1}^n (Q_m - Q_s)_i}{\sum_{i=1}^n Q_{m,i}} \times 100 \quad (3)$$

$$RSR = \frac{\sqrt{\sum_{i=1}^n (Q_{s,i} - Q_{m,i})^2}}{\sqrt{\sum_{i=1}^n (Q_{m,i} - \bar{Q}_m)^2}} \quad (4)$$

$$RMSE = \sqrt{\frac{1}{n} \times \sum_{i=1}^n (Q_{s,i} - Q_{m,i})^2} \quad (5)$$

$$d = 1 - \left[\frac{\sum_{i=1}^n (Q_{s,i} - Q_{m,i})^2}{\sum_{i=1}^n (|Q_{s,i} - \bar{Q}_m| + |Q_{m,i} - \bar{Q}_m|)^2} \right] \quad (6)$$

$$NRMSE = \frac{\sqrt{\frac{1}{n} \sum_{i=1}^n (Q_{s,i} - Q_{m,i})^2}}{\bar{Q}_m} \times 100 \quad (7)$$

$$ME = \frac{1}{n} \left[\sum_{i=1}^n (Q_{s,i} - Q_{m,i}) \right] \quad (8)$$

$$KGE = 1 - \sqrt{(r - 1)^2 + (\beta - 1)^2 + (\gamma - 1)^2} \quad (9)$$

where Q_s is simulation value; Q_m is actual measurement value; n is the number of actual measurements; \bar{Q}_s and \bar{Q}_m are mean values of simulation values and actual measurements, respectively; r is the linear correlation between simulation values and observed values; and β is the specific value between simulation value and observed value.

Appendix B. Supplementary material

Supplementary data to this article can be found online at <https://doi.org/10.1016/j.compag.2022.107408>.

References

- Aghsaee, H., Mobarghaee Dinan, N., Moridi, A., Asadolahi, Z., Delavar, M., Fohrer, N., Wagner, P.D., 2020. Effects of dynamic land use/land cover change on water resources and sediment yield in the Anzali wetland catchment, Gilan, Iran. *Science of the Total Environment* 712, 136449.
- Allen, R.G., Pereira, L.S., Raes, D., Smith, M., 1998. Crop Evapotranspiration-Guidelines for Computing Crop Water Requirements-FAO Irrigation and Drainage Paper No. 56. Rome.
- Arnold, J.G., Srinivasan, R., Muttiah, R.S., Williams, J.R., 1998. Large area hydrologic modeling and assessment Part I: Model Development. *Journal of the American Water Resources Association* 34 (1), 73–89. <https://doi.org/10.1111/j.1752-1688.1998.tb05961.x>.
- Chen, Y., Marek, G.W., Marek, T.H., Brauer, D.K., Srinivasan, R., 2018. Improving SWAT auto-irrigation functions for simulating agricultural irrigation management using long-term lysimeter field data. *Environmental Modelling & Software* 99, 25–38. <https://doi.org/10.1016/j.envsoft.2017.09.013>.
- Chen, Y., Marek, G.W., Mark, T.H., et al., 2019. Simulating the impacts of climate change on hydrology and crop production in the Northern High Plains of Texas using an improved SWAT model. *Agricultural Water Management* 221, 13–24. <https://doi.org/10.1016/j.agwat.2020.106574>.
- Chen, Y., Marek, G.W., Marek, T.H., Porter, D.O., Moorhead, J.E., Heflin, K.R., Brauer, D. K., Srinivasan, R., 2020. Watershed scale evaluation of an improved SWAT auto-irrigation function. *Environmental Modelling & Software* 131, 104789. <https://doi.org/10.1016/j.envsoft.2020.104789>.
- Cotterman, K.A., Kendall, A.D., Basso, B., Hyndman, D.W., 2018. Groundwater depletion and climate change: future prospects of crop production in the Central High Plains Aquifer. *Climatic Change* 146 (1–2), 187–200. <https://doi.org/10.1007/s10584-017-1947-7>.
- Darbandsari, P., Coulibaly, P., 2020. Inter-comparison of lumped hydrological models in data-scarce watersheds using different precipitation forcing data sets: Case study of Northern Ontario, Canada. *Journal of Hydrology: Regional Studies* 31, 100730. <https://doi.org/10.1016/j.ejrh.2020.100730>.
- Deryng, D., Elliott, J., Folberth, C., Muller, C., Pugh, T.A.M., Boote, K.J., Conway, D., Ruane, A.C., Gerten, D., Jones, J.W., Khabarov, N., Olin, S., Schapho, S., Schmid, E., Yang, H., Rosenzweig, C., 2016. Regional disparities in the beneficial effects of rising CO₂ concentrations on crop water productivity. *Nature Climate Change* 6 (8), 786–790. <https://doi.org/10.1038/NCLIMATE2995>.
- Gassman, P.W., Sadeghi, A.M., Srinivasan, R., 2014. Applications of the SWAT model special section: overview and insights. *Journal of Environmental Quality* 43, 1–8. <https://doi.org/10.2134/jeq2013.11.0466>.
- Gupta, H.V., Kling, H., Yilmaz, K.K., Martinez, G.F., 2009. Decomposition of the mean squared error and NSE performance criteria: Implications for improving hydrological modelling. *Journal of Hydrology* 377 (1), 80–91. <https://doi.org/10.1016/j.jhydrol.2009.08.003>.
- Hamed, M.M., Nashwan, M.S., Shahid, S., Ismail, T.B., Wang, X.-J., Dewan, A., Asaduzzaman, M.d., 2022. Inconsistency in historical simulations and future projections of temperature and rainfall: A comparison of CMIP5 and CMIP6 models over Southeast Asia. *Atmospheric Research* 265, 105927.
- Hickman, G.C., Vanloocke, A., Dohleman, F.G., Bernacchi, C.J., 2010. A comparison of canopy evapotranspiration for maize and two perennial grasses identified as potential bioenergy crops. *Global Change Biology Bioenergy* 2 (4), 157–168. <https://doi.org/10.1111/j.1757-1707.2010.01050.x>.
- Holzworth, D.P., Snow, V., Janssen, S., Athanasiadis, I.N., Donatelli, M., Hoogenboom, G., White, J.W., Thorburn, P., 2015. Agricultural production systems modelling and software: current status and future prospects. *Environmental Modelling and Software* 72, 276–286. <https://doi.org/10.1016/j.envsoft.2014.12.013>.
- IPCC, 2014. Climate Change 2013: The Physical Science Basis. Contribution of Working Group I to the Fifth Assessment Report of the Intergovernmental Panel on Climate Change. Cambridge University Press, Cambridge.
- IPCC, 2015. Climate Change 2014: Impacts, Adaptation, and Vulnerability Part B: Regional Aspects. Contribution of Working Group II to the Fifth Assessment Report of the Intergovernmental Panel on Climate Change. Cambridge University Press, Cambridge.
- Jia, S.F., Jiang, W.L., Shen, D.J., 2006. Science of Water Resource Economic. China Water&Power Press, Beijing (in Chinese).
- Jones, C., Robertson, E., Arora, V., Friedlingstein, P., Shevliakova, E., Bopp, L., Brovkin, V., Hajima, T., Kato, E., Kawamiya, M., Liddicoat, S., Lindsay, K., Reick, C. H., Roelandt, C., Segsneider, J., Tjiputra, J., 2013. Twenty-first-century compatible CO₂ emissions and airborne fraction simulated by CMIP5 earth system models under four representative concentration pathways. *Journal of Climate* 26 (13), 4398–4413. <https://doi.org/10.1175/JCLI-D-12-00554.1>.
- Kim, D.H., Jang, T., Hwang, S., 2020. Evaluating impacts of climate change on hydrology and total nitrogen loads using coupled APEX-paddy and SWAT models. *Paddy and Water Environment* 18 (3), 515–529. <https://doi.org/10.1007/s10333-020-00798-4>.
- Kim, H.K., Parajuli, P.B., Filip To, S.D., 2013. Assessing impacts of bioenergy crops and climate change on hydrometeorology in the Yazoo River Basin, Mississippi. *Agricultural and Forest Meteorology* 169, 61–73. <https://doi.org/10.1016/j.agrformet.2012.10.007>.
- Kumar, N., Singh, S.K., Srivastava, P.K., Narsimlu, B., 2017. SWAT Model calibration and uncertainty analysis for streamflow prediction of the Tons River Basin, India, using Sequential Uncertainty Fitting (SUFI-2) algorithm. *Modeling Earth Systems and Environment* 3 (1). <https://doi.org/10.1007/s40808-017-0306-z>.
- Kumari, N., Srivastava, A., Sahoo, B., Raghuvanshi, N.S., Bretreger, D., 2021. Identification of Suitable Hydrological Models for Streamflow Assessment in the Kangsabati River Basin, India, by Using Different Model Selection Scores. *Natural Resources Research* 30 (6), 4187–4205.
- Li, D., Feng, M.Q., Bai, J.Z., Gou, T., 2016. SWAT model based simulation of non-point source pollution for Yuncheng section of Fen river. *Journal of Northwest A & F*

- University (Natural Science Edition) 44 (11), 111–118. [10.13207/j.cnki.jnwafu.2016.11.016](https://doi.org/10.13207/j.cnki.jnwafu.2016.11.016).
- Li, J.Z., Ma, Q.S., Tian, Y., Lei, Y.M., Zhang, T., Feng, P., 2019. Flood scaling under nonstationarity in Daqinghe River basin. *China. Natural Hazards* 98 (2), 675–696. <https://doi.org/10.1007/s11069-019-03724-y>.
- Liu, D.L., O'Leary, G.J., Christy, B., Macadam, L., Wang, B., Anwar, M.R., Weeks, A., 2017. Effects of different climate downscaling methods on the assessment of climate change impacts on wheat cropping systems. *Climatic Change* 144 (4), 687–701. <https://doi.org/10.1007/s10584-017-2054-5>.
- Liu, D.L., Zuo, H.P., 2012. Statistical downscaling of daily climate variables for climate change impact assessment over New South Wales. *Australia. Climatic Change* 115 (3–4), 629–666. <https://doi.org/10.1007/s10584-012-0464-y>.
- Lobell, D.B., Schlenker, W., Costa-Roberts, J., 2011. Climate Trends and Global Crop Production Since 1980. *Science* 333(6042), 616–620. <https://doi.org/10.1126/science.1204531>.
- Marek, G.W., Gowda, P.H., Marek, T.H., Porter, D.O., Baumhardt, R.L., Brauer, D.K., 2017. Modeling long-term water use of irrigated cropping rotations in the Texas High Plains using SWAT. *Irrigation Science* 35 (2), 111–123. <https://doi.org/10.1007/s00271-016-0524-6>.
- Marek, G.W., Baumhardt, R.L., Brauer, D.K., et al., 2018. Evaluation of the Oceanic Nino Index as a decision support tool for winter wheat cropping systems in the Texas High Plains using SWAT. *Computer and Electronics in Agriculture* 151, 331–337. <https://doi.org/10.1016/j.compag.2018.06.030>.
- McGuire, S., 2015. FAO, IFAD, and WFP. The state of food insecurity in the world 2015: meeting the 2015 international hunger targets: taking stock of uneven progress. Rome: FAO, 2015. *Advances in Nutrition* 6(5), 623–624. <https://doi.org/10.3945/an.115.009936>.
- Medlyn, B.E., Barton, C.V.M., Broadmeadow, M.S.J., Ceulemans, R., De Angelis, P., Forstreuter, M., Freeman, M., Jackson, S.B., Kellomäki, S., Laitat, E., Rey, A., Roberntz, P., Sigurdsson, B.D., Strassmeyer, J., Wang, K., Curtis, P.S., Jarvis, P.G., 2001. Stomatal conductance of forest species after long-term exposure to elevated CO₂ concentration: a synthesis. *New Phytologist* 149(2), 247–264. <https://doi.org/10.1046/j.1469-8137.2001.00028.x>.
- Meinshausen, M., Smith, S.J., Calvin, K., Daniel, J.S., Kainuma, M.L.T., Lamarque, J.-F., Matsumoto, K., Montzka, S.A., Raper, S.C.B., Riahi, K., Thomson, A., Velders, G.J.M., van Vuuren, D.P.P., 2011. The RCP greenhouse gas concentrations and their extensions from 1765 to 2300. *Climatic Change* 109 (1–2), 213–241.
- Mirsafi, Z.S., Sepaskhah, A.R., Ahmadi, S.H., Kamgar-Haghighi, A.A., 2016. Assessment of AquaCrop model for simulating growth and yield of saffron (*Crocus sativus* L.). *Scientia Horticulturae* 211, 343–351. <https://doi.org/10.1016/j.scienta.2016.09.020>.
- Phong, V.V., Le, P.K., Darren, T.D., 2011. Implications for the hydrologic cycle under climate change due to the expansion of bioenergy crops in the Midwestern United States. *Proceedings of the National Academy of Sciences of the United States* 108 (37), 15085–15090. <https://doi.org/10.1073/pnas.1107177108>.
- Piao, S.L., Ciais, P., Huang, Y., Ciais, P., Huang, Y., Shen, Z.H., Peng, S.S., Li, J.S., Zhou, L.P., Liu, H.Y., Ma, Y.C., Ding, Y.H., Friedlingstein, P., Liu, C.Z., Tan, K., Yu, Y. Q., Zhang, T.Y., Fang, J.Y., 2010. The impacts of climate change on water resources and agriculture in China. *Nature* 467 (7311), 43–51. <https://doi.org/10.1038/nature09364>.
- Pritchard, S.G., Prior, S.A., Peterson, C.M., Rogers, H.H., 1999. Elevated CO₂ and plant structure: a review. *Global Change Biology* 5 (7), 837. <https://doi.org/10.1046/j.1365-2486.1999.00268.x>.
- Song, Y.H., Chung, E.S., Shahid, S., 2021. Spatiotemporal differences and uncertainties in projections of precipitation and temperature in South Korea from CMIP6 and CMIP5 general circulation models. *International Journal of Climatology* 41 (13), 5899–5919. <https://doi.org/10.1002/joc.7159>.
- Sreeharsha, R.V., Sekhar, K.M., Reddy, A.R., 2015. Delayed flowering is associated with lack of photosynthetic acclimation in Pigeon pea (*Cajanus cajan* L.) grown under elevated CO₂. *Plant Science* 231, 82–93.
- Srivastava, A., Kumari, N., Maza, M., 2020. Hydrological response to agricultural land use heterogeneity using variable infiltration capacity model. *Water Resource Management* 34 (12), 3779–3794. <https://doi.org/10.1007/s11269-020-02630-4>.
- Stocker, T., 2014. *Climate change 2013: the physical science basis: Working Group I contribution to the Fifth assessment report of the Intergovernmental Panel on Climate Change*. Cambridge University Press.
- Tan, L.L., Feng, P.Y., Li, B.G., Huang, F., Liu, D.L., Ren, P.P., Liu, H.P., Srinivasan, R., Chen, Y., 2022. Climate change impacts on crop water productivity and net groundwater use under a double-cropping system with intensive irrigation in the Haihe River Basin. *China. Agricultural Water Management* 266, 107560. <https://doi.org/10.1016/j.agwat.2022.107560>.
- Tao, F.L., Yokozawa, M., Liu, J.Y., Zhang, Z., 2008. Climate-crop yield relationships at provincial scales in China and the impacts of recent climate trends. *Climate Research* 38 (1), 83–94. <https://doi.org/10.3354/cr00771>.
- Taylor, K.E., 2001. Summarizing multiple aspects of model performance in a single diagram. *Journal of Geophysical Research-Atmospheres* 106 (D7), 7183–7192. <https://doi.org/10.1029/2000JD900719>.
- Taylor, K.E., Stouffer, R.J., Meehl, G.A., 2012. An overview of CMIP5 and the experiment design. *Bulletin of the American Meteorological Society* 93 (4), 485–498. <https://doi.org/10.1175/BAMS-D-11-00094.1>.
- Teixeira, E.I., Ruiten, J.D., Ausseil, A.G., Daigneault, A., Johnstone, P., Holmes, A., Tait, A., Ewert, F., 2018. Adapting crop rotations to climate change in regional impact modelling assessments. *Science of the Total Environment* 616, 785–795. <https://doi.org/10.1016/j.scitotenv.2017.10.247>.
- Van Vuuren, D., Elzen, M., Lucas, P.L., Eickhout, B., Strengers, B.J., Ruijven, B.V., Wonink, S., Houdt, R.V., 2007. Stabilizing greenhouse gas concentrations at low levels: an assessment of reduction strategies and costs. *Climatic Change* 81 (2), 119–159. <https://doi.org/10.1007/s10584-006-9172-9>.
- van Vuuren, D.P., Stehfest, E., den Elzen, M.G.J., Kram, T., van Vliet, J., Deetman, S., Isaac, M., Klein Goldewijk, K., Hof, A., Mendoza Beltran, A., Oosterrijk, R., van Ruijven, B., 2011. RCP2.6: exploring the possibility to keep global mean temperature increase below 2°C. *Climatic Change* 109 (1–2), 95–116.
- Wand, S.J.E., Midgley, G.F., Jones, M.H., Curtis, P.S., 1999. Responses of wild C₄ and C₃ grass (*Poaceae*) species to elevated atmospheric CO₂ concentration: a meta-analytic test of current theories and perceptions. *Global Change Biology* 5 (6), 723–741.
- Wang, Q., Qi, J., Li, J., Cole, J., Waldhoff, S.T., Zhang, X., 2020. Nitrate loading projection is sensitive to freeze-thaw cycle representation. *Water Research* 186, 116355. <https://doi.org/10.1016/j.watres.2020.116355>.
- Wang, X.L., Xu, S.H., Li, Y.X., Cui, D.C., 1995. Responses of Growth and Development, physiology and yield of Maize to Increasing CO₂ Concentration. *Transactions of the Chinese Society of Agricultural Engineering* 02, 109–114.
- Wang, X.L., Xu, S.H., Liang, H., 1998. The experimental study of the effects of CO₂ concentration enrichment on growth, development and yield of C₃ and C₄ crops. *Scientia Agricultura Sinica* 31 (1), 55–61. <https://doi.org/10.3321/j.issn:0578-1752.1998.01.009>.
- Willmott, C.J., 1982. Some comments on the Evaluation of Model Performance. *Bulletin of the American Meteorological Society* 63(11), 1309–1313. [https://doi.org/10.1175/1520-0477\(1982\)063<1309:SCOTEO>2.0.CO;2](https://doi.org/10.1175/1520-0477(1982)063<1309:SCOTEO>2.0.CO;2).
- Wu, Y., Liu, S., 2012. Impacts of biofuels production alternatives on water quantity and quality in the Iowa River Basin. *Biomass and Bioenergy* 36, 182–191. <https://doi.org/10.1016/j.biombioe.2011.10.030>.
- Wu, Y., Liu, S., Abdul-Aziz, O.I., 2012. Hydrological effects of the increased CO₂ and climate change in the Upper Mississippi River Basin using a modified SWAT. *Climatic Change* 110 (3–4), 977–1003. <https://doi.org/10.1007/s10584-011-0087-8>.
- Wu, T., Lu, Y., Fang, Y., Xin, X., Li, L., Li, W., Jie, W., Zhang, J., Liu, Y., Zhang, L., Zhang, F., Zhang, Y., Wu, F., Li, J., Chu, M., Wang, Z., Shi, X., Liu, X., Wei, M., Huang, A., Zhang, Y., Liu, X., 2019. The Beijing Climate Center Climate System Model (BCC-CSM): the main progress from CMIP5 to CMIP6. *Geoscientific Model Development* 12 (4), 1573–1600.
- Xiao, D., Liu, D.L., Wang, B., Feng, P., Bai, H., Tang, J., 2020. Climate change impact on yields and water use of wheat and maize in the North China Plain under future climate change scenarios. *Agricultural Water Management* 238, 106238. <https://doi.org/10.1016/j.agwat.2020.106238>.
- Xiao, D., Liu, D.L., Feng, P., Wang, B., Waters, C., Shen, Y., Qi, Y., Bai, H., Tang, J., 2021. Future climate change impacts on grain yield and groundwater use under different cropping systems in the North China Plain. *Agricultural Water Management* 246, 106685.
- Xiao, D., Tao, F., 2014. Contributions of cultivars, management and climate change to winter wheat yield in the North China Plain in the past three decades. *European Journal of Agronomy* 52, 112–122. <https://doi.org/10.1016/j.eja.2013.09.020>.
- Xiong, W., Holman, I., Lin, E., Conway, D., Jiang, J., Xu, Y., Li, Y., 2010. Climate change, water availability and future cereal production in China. *Agriculture Ecosystems and Environment* 135 (1–2), 58–69.
- Xu, Z.Z., Jiang, Y.L., Jia, B.R., Zhou, G.S., 2016. Elevated-CO₂ response of stomata and its dependence on environmental factors. *Frontiers in Plant Science* 7, 657. <https://doi.org/10.3389/fpls.2016.00657>.
- Zhang, X.L., Ren, L., Feng, W., 2022. Comparison of the shallow groundwater storage change estimated by a distributed hydrological model and GRACE satellite gravimetry in a well-irrigated plain of the Haihe River basin. *China. Journal of Hydrology* 610, 127799. <https://doi.org/10.1016/j.jhydrol.2022.127799>.
- Zhang, X., Wang, S., Sun, H., Chen, S., Shao, L., Liu, X., 2013. Contribution of cultivar, fertilizer and weather to yield variation of winter wheat over three decades: A case study in the North China Plain. *European Journal of Agronomy* 50 (1), 52–59. <https://doi.org/10.1016/j.eja.2013.05.005>.
- Zhu, Y., Yang, S., 2020. Evaluation of CMIP6 for historical temperature and precipitation over the Tibetan Plateau and its comparison with CMIP5. *Advance in Climate Change Research* 11 (3), 239–251. <https://doi.org/10.1016/j.accre.2020.08.001>.